Qafoku O, Pearce C, Neumann A, Kovarik L, Zhu M, Ilton E, Bowden M, Resch C, Arey B, Arenholz E, Felmy A, Rosso K.

Tc(VII) and Cr(VI) Interaction with a Naturally Reduced Ferruginous Smectite from a Redox Transition Zone.

***Environmental Science & Technology* 2017, 51(16), 9042-9052.**

Tc(VII) and Cr(VI) Interaction with Naturally Reduced Ferruginous Smectite from a Redox Transition Zone

*Odeta Qafoku[1], Carolyn I. Pearce[1], Anke Neumann[2], Libor Kovarik[3], Mengqiang Zhu[4], Eugene S. Ilton[1], Mark E. Bowden[3], Charles T. Resch[1], Bruce W. Arey[3], Elke Arenholz[5], Andrew R. Felmy[1,6], Kevin M. Rosso[1]

[1]Pacific Northwest National Laboratory, P.O. Box 999, MS K8-96, Richland, Washington, 99352, U.S.A.

[2]Newcastle University, Newcastle, U.K.

[3]Environmental Molecular Sciences Laboratory, PNNL, U.S.A.

[4]University of Wyoming, Laramie, Wyoming, U.S.A.

[5]Lawrence Berkeley National Laboratory, Berkeley, California, U.S.A.

[6]Washington State University, Pullman. Washington, U.S.A.

*Corresponding author: odeta.qafoku@pnnl.gov; Phone: + 509-371-6353; Fax: + 509-371-6354.

To be submitted to Environmental Science & Technology

ABSTRACT

Fe(II)-rich clay minerals found in subsurface redox transition zones (RTZs) can serve as important source of electron equivalents limiting the transport of redox active contaminants. While most laboratory reactivity studies are based on reduced model clays, the reactivity of naturally reduced clays in field samples remains poorly explored. Characterization of the clay size fraction of a fine-grained unit from RTZ interface at the Hanford site, Washington, including mineralogy, crystal chemistry, and Fe(II)/(III) content, indicates that ferruginous montmorillonite is the dominant mineralogical component. Oxic and anoxic fractions differ significantly in Fe(II) content, but Fe_{TOTAL} remains constant demonstrating no Fe loss during reduction-oxidation cyclings. At native pH of 8.6 the anoxic fraction despite its significant Fe(II), ~23% of Fe_{TOTAL}, exhibits minimal reactivity with TcO_4^- and CrO_4^{2-} and much slower reaction kinetics than that measured in studies with biologically/chemically reduced model clays. Reduction capacity is enhanced by added/sorbed Fe(II) (if $Fe(II)_{SORBED}$ >8% clay $Fe(II)_{LABILE}$), however the kinetics of this conceptually surface-mediated reaction remain sluggish. Surface-sensitive Fe L-edge X-ray absorption spectroscopy shows that $Fe(II)_{SORBED}$ and the resulting reducing equivalents are not available in the outermost few nanometers of clay surfaces. Slow kinetics thus appear related to diffusion-limited access to electron equivalents retained within clay mineral.

INTRODUCTION

Clay minerals rich in iron play a unique role in biogeochemical and environmental reduction-oxidation (redox) reactions in soils and subsurface environments, acting as a recyclable sink or source of electron equivalents. The structure of clay minerals enables Fe structural to alternate valence between Fe(III) and Fe(II) while charge neutralization mechanisms intrinsic to these materials maintain overall charge balance and phase stability. Consequently, many studies have been devoted to understanding linkages between redox processes occurring in aqueous solution and the Fe(II)/Fe(III) redox couple found in a variety of phyllosilicates from clays to micas. Examples include demonstrating that phyllosilicate structural Fe(III) is an accessible electron acceptor for a wide range of microbial communities[1-4] and that a structural Fe(II) in phyllosilicates can reduce redox-active contaminants.[5-11]

Of particular interest to the present study, the transport of radioactive ^{99}Tc(VII) and toxic Cr(VI) contaminants could be strongly retarded by redox reaction with reduced Fe-clay minerals. These hazardous and problematic subsurface contaminants are typically found at historic nuclear processing facilities, such as the Hanford Nuclear Reservation, USA. In oxic subsurface and groundwater, pertechnetate (TcO_4^-) and chromate (CrO_4^{2-}) are the stable species, and in these forms they are highly mobile due to limited sorption to geomedia at neutral and alkaline environments.[12-17] However, their mobility could substantially decrease if donors capable of reducing Tc and Cr oxyanions to their respective insoluble precipitates $Tc(IV)O_2{\cdot}nH_2O_{(s)}$ ($10^{-8.2}$ mol/L) and $Cr(III)(OH)_3$ (10^{-7} mol/L) are present.[18-20] For Tc(VII) and Cr(VI) reduction, previous research highlights the contrasting importance of homogeneous and heterogeneous pathways. Homogeneous Tc(VII) reduction by aqueous Fe(II) is unlikely at circumneutral pH[19] whereas the rate and the extent of heterogeneous Tc(VII) reduction is increased by $Fe(II)_{SORBED}$

65 or by $Fe(II)_{STRUCTURAL}$ [21]. In contrast, in neutral and basic pH's homogeneous Cr(VI) reduction
66 is nearly instantaneous[17,22-25] while heterogeneous reduction is significantly slower and depends
67 on Fe(II) content in structural sites as well as mineralogy.[17,26-29] Many studies have
68 demonstrated the reduction capacity of Fe(II)-bearing crystalline solids, including iron-rich clay
69 minerals.[7,8,21,22,26-28,30-37] Thus, if Fe(II)-bearing clay minerals are capable of reducing Tc(VII)
70 and Cr(VI), a conceptual model of an Fe-clay rich stratum acting as a natural semi-permeable
71 reactive barrier can be developed; a natural reduction layer that can be episodically recharged
72 with reducing equivalents by seasonal fluctuations in the water table at the redox boundary.

73 To explore this prospect, pathways for electron exchange between reservoirs of Fe within clay
74 minerals and redox-active contaminants need to be better understood. Under reducing conditions,
75 this includes resolving the separate roles of bulk structural Fe(II), edge-bound Fe(II), and
76 interlayer/basal surface exchangeable Fe(II) in heterogeneous electron transfer (ET). The role of
77 associated aqueous Fe(II) that would comprise both a competitive homogeneous reduction
78 pathway and/or a regeneration pathway for mineralogic Fe(II) must also be considered. For
79 example, biogenic Fe(III)-(oxyhydr)oxide reduction produces aqueous Fe(II)[38,39] that can, in
80 turn, sorb strongly onto clay minerals[5,30,40,41] binding to –OH edge complexation sites or basal
81 exchange sites.[34,42-45] This sorbed Fe(II) can exchange electrons with structural Fe(III), primarily
82 via edge-bound sites, with lesser participation from Fe(II) sorbed on basal/interlayer
83 exchangeable sites.[44,46-48] As a result, disentangling the pathways for ET across the Fe-
84 clay/sorbate/solution interface is complicated by these self-exchange dynamics of electrons
85 between structural, sorbed, and aqueous Fe.

86 The present study examines the reduction of Tc(VII) and Cr(VI) by the clay-sized fraction of
87 a fine-grained sediment that is dominated mineralogically by a naturally reduced ferruginous

smectite. The sediment comprises a distinct low permeability lithologic facies that contains the redox transition zone (RTZ) in the Ringold formation at the 300 Area of the Hanford site. Our study is motivated to address several persisting knowledge gaps. First, the majority of bespoke previous work has been performed on reference clay minerals from standard sources, many of which had above average Fe content and/or were prepared in the laboratory using a one-cycle chemical or biological reduction approach outside of a specific environmental context (e.g., up to 100% pre-reduction by dithionite). In one exception[49] a reference clay was subjected to multiple biogenic redox cycles, with each subsequent redox cycle showing accelerated Tc(VII) reduction rates. However, very few studies have been conducted with naturally reduced clays, expectedly distinct both in terms of reduction extent and numbers of redox cycles, which can impact clay mineral reduction potential.[50,51] Thus it is of interest to determine if Fe-rich clays in their native settings follow the same redox behavior as the model analogs. Secondly, we build on prior work[20] that examined a coarser, mixed-mineralogic fraction of an adjacent sediment facies containing the ferruginous clay fraction isolated and studied here. That study indicated that this phase, along with other Fe(II)-bearing mineral phases present, were reactive with Tc(VII). We also build on a recent study[52] which showed negligent reactivity in nitrate bioreduction by the anoxic whole intact sediment of the identical facies ; reactivity that was enhanced by sediment amendment with external bioavailable carbon. Finally, to address reactivity of clay subsequent to surface recharging with reducing equivalents, we explore the role of addition of aqueous Fe(II) to pristine anoxic ferruginous clay with regard to Tc(VII) and Cr(VI) reduction.

MATERIALS AND METHODS

Sediments from core samples were collected from above and below the oxidized-reduced interface in the RTZ at Hanford's 300 Area. These fine sand to silt textured, clay-rich sediments

provided the initial materials for our study, collected from oxic ~ 18.0 – 18.3 m and anoxic ~ 18.6 – 18.9 m sediment profiles that differed sharply in coloration from light brown (oxic) to bluish-gray (anoxic). The stratographic, geochemical, mineralogic, and microbial characteristics of whole sediments and size fraction < 5 mm have been described elsewhere.[20,53,54] In this study we characterized < 2 μm size fraction.

Isolation and preparation of the clay-sized fraction. Prior to size fractionation, the oxic sediment was dried in air while the anoxic sediment was dried in a N_2 chamber (P_{O2} <0.1 ppm). All procedures with the naturally reduced material were performed inside this chamber with N_2 degassed solutions. After gentle crushing, the sediments were passed through a sieve (0.5 mm size) with no remaining fraction above this size. Alteration of natural cation distribution was minimized by dispersing the materials via sonication in deionized water. Fractionation to clay-sized particles (< 2 μm) was completed by sedimentation[55] under gravity (Supporting Information, S1). Samples were freeze-dried and BET (Brunauer-Emmett-Teller) specific surface areas were determined by measuring N_2 adsorption isotherms.[56]

X-ray diffraction (XRD). The mineralogies of the oxic and anoxic clay fractions were determined by XRD using a Philips X'Pert MPD system with a vertical goniometer on randomly oriented powder mounts, with an internal standard (ZnO) for phase quantification. Individual clay minerals were identified in oriented specimens after oxic clay was equilibrated with Mg- and K- solutions[55] (Supporting Information, S2-S3).

Chemical Characterization. Total chemical composition, including Fe(II)/(III) speciation, was determined by HF-H_2SO_4 acid digestion in the presence of 1, 10-phenanthroline monohydrate as the chromophore[57] (Supporting Information, S4). Further characterization

included cation exchange capacity, exchangeable cations, Fe(II) most reactive fraction[20], Fe crystalline component, and inorganic C (Supporting Information, S5). Chemical and mineralogical data was used to derive an approximate clay structural unit full-cell formula assuming that the ideal clay formula consists of 44 positive charges (Table 1). Further, the extent of reduction in native oxic clay was determined using anthraquinone-2,6-disulfonic acid (AQDS/AH_2DS) as an electron source (Supporting Information, S6).

Spectroscopic and microscopic analyses. Clay samples were characterized by a combination of spectroscopic and microscopic techniques as follows.

Fe K-edge extended X-ray absorption fine structure spectra with linear combination fitting (EXAFS/LCF) analysis were collected from clay samples in transmission mode at beamline 4-3 equipped with a Si (111) monochromator (Stanford Synchrotron Radiation Lightsource, Menlo Park, CA). EXAFS/LCF analysis was used for data fitting with spectra of known Fe-containing solids summed at certain proportions to match sample spectra (Supporting Information, S7).

Fe L-edge X-ray absorption spectroscopy (XAS) and X-ray magnetic circular dichroism (XMCD) data for oxic and anoxic samples were measured on beamline 4.0.2 at the Advanced Light Source (ALS) in Berkeley, California, using the eight-pole resistive magnet end station[55]. The XAS signal was monitored in total-electron-yield (TEY) mode with an effective probing depth of ~4.5 nm. The experimental spectra (Supporting Information, S7) were normalized with respect to the background so that the L_3 main peak intensity was equal to 1.

Mössbauer spectra of clay samples were collected at room temperature and 14 K for the oxic fraction and at 18 K for the anoxic fraction (Supporting Information, S9). The spectra were

154 measured in transition mode with constant acceleration on a spectrometer supplied by Web
155 Research, Inc. and equipped with a closed-cycle cryostat (CCS-850 System, Janis Research Co.)

156 Scanning electron microscopy (SEM) analyses were performed on Quanta 3D FEG equipped
157 with an energy-dispersive X-ray detector (EDS) for semiqualitative analysis at an acceleration
158 voltage of 20 kV. High resolution transmission electron microscopy (TEM) analyses were
159 performed on a Jeol-JEM microscope with operating voltage of 200 kV. TEM specimens from
160 post-reacted samples were prepared using field emission focused ion beam FIB-SEM, Helios 600
161 (Supporting Information, S10).

162 **Tc(VII) and Cr(VI) batch reduction.**

163 *Interaction with the anoxic clay alone.* Anoxic clay fraction was used to investigate Tc(VII)
164 and Cr(VI) reduction over a 2 month period. The freeze-dried clay was suspended in de-ionized
165 water to perserve native cation distribution. A density of 9 g/L was selected consistent with a
166 study that investigated the reactivity of coarser fraction (< 0.5 mm) of RTZ anoxic sediment.[20]
167 The pH was allowed to equilibrate to the natural buffering capacity of the sediment, ~ 8.6.
168 Reduction experiments, in triplicates, were conducted at 2.5 μM and 10 μM for Tc(VII) and, 2.5
169 μM and 50 μM for Cr(VI) (Supporting Information, S11).

170 *Interaction with the anoxic clay augmented with aqueous Fe(II).* A second set of
171 experiments identical to those described were performed after anoxic clay suspensions were pre-
172 equilibrated with aqueous Fe(II) for 0.5 h; respectively with 10 μM aqueous Fe(II) prior to
173 addition of 2.5μM Tc(VII) or Cr(VI), 30 μM aqueous Fe(II) prior to addition of 10 μM Tc(VII),
174 and 150 μM aqueous Fe(II) prior to addition of 50 μM Cr(VI). Experiments were conducted at
175 conditions nominally undersaturated with respect to $Fe(OH)_2$; for verification control

176 experiments in the absence of clay were also carried out. Following $FeCl_2$ addition, and
177 preceding Cr(VI) and Tc(VII) spikes, clay suspensions were analyzed for Fe(II) using ferrozine
178 method[59]. Selected post-reaction solids including a precipitate from homogeneous reaction 150
179 μM Fe(II) / 30 μM Cr(VI) at pH 8, were characterized with SEM/EDS, XAS, and FIB-TEM.
180 Following 0.5 h Fe(II) sorption experiments, a series of extractions were performed on clay
181 suspensions to probe sorbed Fe(II); these included extraction in NaCl, $CaCl_2$, $MgCl_2$, NaH_2PO_4,
182 NH_4-acetate, and HCl at pH ~4. The extracting solutions aimed to differentiate whether sorbed
183 Fe(II) was bound to basal/interlayer exchangeable sites, OH-complexation sites or precipitated as
184 Fe-hydroxide.

185 **RESULTS**

186 **RTZ clay characterization**

187 *Bulk Mineralogy.* Particle size fractionation of oxic and anoxic RTZ sediments reveals that
188 the clay sized fraction (< 2 μm) accounts for 6.1 and 8.6% of sediments by mass, respectively
189 (Table S1). The mineralogy of the two clay fractions is very similar, as shown by XRD analysis
190 (Figure S1), and is dominated by the clay minerals, smectite and kaolinite. The smectite
191 component (82-84%) was calculated based on the difference from the other mineral components
192 (kaolinite, albite, quartz, anorthoclase, and cristobalite) quantified by Rietveld refinement with
193 ZnO as the added standard. The XRD background implies presence of an amorphous component
194 that is more significant in anoxic sample. Citrate/ascorbate (Fe_{ca}) chemical extraction combined
195 with post-extraction XRD analysis (data not shown) demonstrates only minor quantities of
196 poorly crystalline Fe oxides (Fe_{ca} < 1% Fe_{TOTAL}, Table 1). The amorphous component is
197 therefore likely a silica-based by-product of reductive dissolution, a process that can be expected

198 to have been more prevalent in the anoxic sediments. In general, the mineralogy is similar to
199 that described in previous research for coarser fractions of the Hanford 300 Area sediments.[20,60]

200 *Chemical composition and phase identification.* The RTZ oxic and anoxic clay fractions
201 have similar properties and composition with respect to total Fe content, type and concentration
202 of exchangeable cations, CEC, and surface area (Table 1). The major difference is the
203 significantly higher Fe(II) content in the anoxic clay fraction (22.4% of Fe_{TOTAL}); yet it appears
204 that clay reduction events did not result in a net loss of Fe, as the Fe_{TOTAL} is similar for the two
205 fractions. We observed that the maximum reducible Fe by AH_2DS in oxidized clay
206 approximates to 24% Fe(II)/Fe_{TOTAL} (Table S2), effectively the same proportion of Fe(II) as
207 found in native anoxic clay. Furthermore, results suggest that Fe(II) in the anoxic clay is not
208 present as an exchangeable cation (Table 1). Based on 1 h, 0.5 M HCl extraction data, nearly
209 15% of Fe(II) solid-bound species are in the most reactive fraction.[20,37] This fraction represents
210 the contribution from both Fe(II) bound to siloxane edge sites and structural Fe(II), as some
211 dissolution of ultrafine grained silicate minerals had occurred (~ 1% of total Si dissolved, data
212 not shown). However, there is no contribution from $FeCO_3$ (siderite) as the inorganic C content
213 in the clay fraction is insignificant (Table 1). The clay mineral unit cell formula (Table 1),
214 estimated from the chemical composition after accounting for the impurities identified by XRD
215 (Figure S1, Table S1), is representative of a dioctahedral smectite (owing to d_{060} 62° 2θ
216 reflection) and more specifically a montmorillonite (based on the extent of expansion in the d_{001}
217 spacing[60], Table S4) with predominantly Ca and K, and minor Mg and Na, in
218 interlayer/exchangeable basal sites. Compositional and structural data identify the clay mineral
219 in both RTZ oxic and anoxic horizons as ferruginous montmorillonite, with the origin of the
220 layer charge primarily in the octahedral sheet, where Mg and Fe substitute for Al.

221 *Microscopic characterization.* Backscattering SEM images of oxic and anoxic samples
222 display typical 100-200 μm clay aggregates (Figure S2). Clay aggregates from the anoxic
223 horizon also contain several 0.4 to 1.2 μm high Z-contrast crystallites, with equant cubic to
224 octahedral morphologies incorporated into the matrix. Local EDS and elemental distributions
225 mapping in these areas revealed particles composed of Fe and S, with Fe:S ratio that varies from
226 1:1.6 for cubic to 1:1.1 for octahedral crystals. Collectively, from SEM data the sulfide particles
227 in anoxic samples are a minor component below the detection limit for XRD quantitative
228 analysis. By far, the largest reservoir of Fe(II) in the anoxic clay fraction is associated with the
229 clay particles.

230 *Fe K-edge (EXAFS), Fe L-edge (XAS/XMCD), and Mössbauer Spectroscopy.* Fe *K*-edge
231 EXAFS/LCF analysis on the oxic and anoxic clay was performed to further characterize local Fe
232 coordination environment (Figure S3, Table S5). The key observation from EXAFS analysis is
233 that the two clay samples have quite similar Fe local atomic structures and although within the
234 margin of error of the XAFS measurements, the data may possibly indicate a difference in the Fe
235 oxidation state, (Figure S4, Table S6), . Comparison of Fe *L*-edge XAS performed on the oxic
236 RTZ clay (~1.3 mmol/g Fe) and on a Fe-rich reference clay mineral, nontronite NAu-2 (4
237 mmol/g Fe), suggest similar Fe site symmetry and valence (Figure S5, panel a). XAS fitting and
238 normalization of data to Fe_{TOTAL} of 1.33 gives 0.06 Fe(II) and 1.27 Fe(III) in octahedral
239 coordination (Figure S5, panel b). For the anoxic RTZ clay, XAS analysis reveals a slightly more
240 reduced state than nontronite NAu-2 exposed to sufficient sodium dithionite to reduce ~10% of
241 the Fe^{62} (Figure S5, panel c). Fitting the XAS for the anoxic clay (Figure S5, insert d) and
242 normalizing the data to an Fe_{TOTAL} of 1.33 gives 0.28 Fe(II) and 1.05 Fe(III) in octahedral
243 coordination, resulting in a value of 21% Fe(II). The XAS spectra for both the oxic and anoxic

clay show no evidence for Fe in tetrahedral coordination, and the obtained values for Fe(II) and Fe(III) are very similar to that determined by chemical composition analysis (Table 1).

Mössbauer spectra obtained for the oxic and anoxic clays at 18 K showed that magnetically ordered Fe phases such as Fe-(oxyhydr)oxides, sulfides or carbonates, which would appear as sextets, were below the detection limit of 1-2% Fe.[63] The oxic clay fraction (Figure S6, panel A) exhibited one large doublet around 0.5 mm/s, consistent with the presence of octahedral Fe(III) in a non-magnetically ordered environment such as a clay mineral, and the absence of detectable tetrahedral Fe. Similarly, the low temperature Mössbauer spectrum of the reduced clay fraction showed no indication of tetrahedral Fe (Figure S6, panel B). Furthermore, the fit yielded the same Fe(III) and Fe(II) components with almost identical hyperfine parameters, suggesting that the clays are very similar in their Fe mineral composition and binding environments. In contrast to the oxic clay, the octahedral Fe(II) component in the anoxic clay comprised almost 18% of the spectral area. Because the spectral component of the distorted octahedral Fe(III) in the anoxic clay is the same as in the oxic clay, regular octahedral Fe(III) sites were the most likely sites for reduction, accounting for the increase in octahedral Fe(II) in the anoxic clay.

Tc(VII) and Cr(VI) reduction by pristine and Fe(II) augmented anoxic clay

Interaction with pristine anoxic clay. Tc(VII) and Cr(VI) reduction, measured by loss from solution from the point of initial contact with the anoxic clay until ~ 50 d, showed sluggish kinetics overall, with barely significant amounts of Tc(VII) reduction and slow linear Cr(VI) reduction (Figure 1,a-c). Yet, experimental solid to solution ratio and the concentrations of oxyanions were selected to ensure an excess of the most reactive Fe(II), based on 0.5M HCl

extraction (Table 1), by more than a factor of three. To illustrate, reduction of Tc(VII) by the anoxic clay from solutions containing 2.5 μM or 10 μM (data not shown) after ~ 50 d was limited to < 6%, (no significant differences in Tc(VII) reduction were observed among two Fe(II) amendments). In contrast, reduction of 2.5 μM Cr(VI) solution was ~ 46% after 50 d while at the higher concentration of 50 μM, ~ 23% Cr(VI) was reduced (Figure 1,b-c). At the termination of the experiments, no Cr species associated with the reacted clay particles were detected by SEM/EDS analysis. However, Fe *L*-edge XAS analysis showed a decrease in intensity on the low energy side of Fe L_3 peak after clay reaction with 50μM Cr(VI) (Figure 2A) suggesting Cr(VI) loss from solution due to reduction, coupled to oxidation of near surface Fe(II). Overall, despite the substantial excess of Fe(II), the pristine anoxic RTZ clay fraction displayed only very limited capacity for Tc(VII) removal, and a more significant but kinetically slow capacity for Cr(VI) removal from solution (Figure 1, b-c). Within the errors of measurements, the kinetics of Cr(VI) removal displayed similar trends at low, 2.5 μM, and high, 50 μM, concentrations.

Fe(II) uptake by the anoxic clay. Addition of 10, 30, or 150 μM $FeCl_2$ to the anoxic clay suspension resulted in the removal of Fe(II) down to detection limit, presumably by sorption, within 0.5 h of equilibration consistent with literature-based precedent[44-46,64,65] (Table 2, columns 3&4). After adjusting for pH change, sorption of 150 μM $FeCl_2$ or ~33 μmol(reducing)equivalents/g_clay from solution was followed by the release of ~ 21 μmolequivalents/g_clay exchangeable cations from interlayer sites, respectively Ca^{2+}, K^{+}, and Mg^{2+} (Table 2, columns 4&5). This implies that remaining fraction of Fe(II) ~12 μmolequivalents/g_clay, was sorbed onto clay edge sites, which at experimental pH have the largest affinity for iron but limited capacity.[34,44] Indeed, experiments conducted at 10 μM Fe(II)

show that concentration of exchangeable cations before and after Fe sorption were nearly equal (within 1 standard deviation), indicating that sorption at edge sites preceded that of exchangeable sites (Table 2, columns 2&3). The release of exchangeable cations in the order of Ca>K>Mg from clay interlayer/exchangeable sites, is indicative that Fe(II) largely sorbed into clay sites and not on organic C species, whose presence in < 2 μm fraction of Hanford sediment is very low and ineffective in reducing NO^-_3 in prior work[52,53]. Overall, these results indicate that ~ 2/3 of Fe(II) was exchanged for interlayer and basal sites while ~ 1/3 of Fe(II) was likely sorbed into edge sites. We further investigated the actual partitioning of Fe(II), using a series of extractions (Table 2, columns 6-8), selected as follows. The monovalent cation Na^+ was selected to probe cation exchange reactions that could occur upon addition of Na_2CrO_4 during subsequent reactivity experiments. The divalent cations Ca^{2+} and Mg^{2+}, and the complex cation NH_4^+ were selected based on their ability to exchange with Fe(II) sorbed onto clay basal planes. Finally, NaH_2PO_4 was chosen to target Fe(II) sorbed on edge sites.[44] Despite the nature of extracting solutions, little or no Fe(II) was released into solution after 24h equilibration (Table 2) demonstrating that Fe(II) sorbed by the anoxic clay was not exchangeable. Even more perplexing, Fe *L*-edge XAS analysis revealed that no significant change in oxidation state of Fe in the clay occurred after exposure to 150 μM Fe(II) compared to the pristine anoxic clay (Figure 2B). This result likely indicates that, after sorption, the Fe(II) redox-active component was not localized at near surface within the ~5 nm probing depth of *L*-edge XAS but possibly stored within clay interiors (bulk). Even so, Fe(II) augmented clay was more reactive with Cr(VI) than the pristine anoxic clay, as is shown in subsequent reduction experiments.

Interaction with the anoxic clay augmented with Fe(II)aqueous. The reduction capacity of anoxic clay fraction augmented with sorbed Fe(II) was contingent on the type of the contaminant

and on the amount of $Fe(II)_{SORBED}$ (Figure 1,d-f). Compared to reduction by anoxic clay alone, the reduction of 2.5 μM and 10 μM Tc(VII) (data not shown) increased only marginally, by ~2% for 10 μM Fe(II) added (Figure 1,d) and by 6% for 30μM Fe(II) added (data not shown). Likewise, reduction of 2.5 μM Cr(VI) increased by ~3% for 10 μM $Fe(II)_{SORBED}$ (Figure 1,e). However, the redox capacity of anoxic clay augmented with 150 μM Fe(II) was enhanced considerably, as indicated by near complete reduction of 50 μM Cr(VI) at ~50d (Figure 1f). Solid post-reaction SEM/EDS mapping revealed formation of high Z-contrast micron-size discrete particles with a non-specific morphology, rich in Cr and Fe (Figure 3). Examination by FIB-TEM indicated that these particles were composed of individual 10-50 nm crystallites, with electron diffraction showing a ring pattern corresponding to an ensemble of randomly oriented crystallites (Figure S7). Despite substantial reduction, Cr concentration was too low to obtain a Cr *L*-edge XAS spectrum. The Fe *L*-edge XAS of the anoxic clay pre-equilibrated with 150μM Fe(II) before and after reaction with 50 μM Cr(VI) showed no change in Fe oxidation state (Figure 2,C), suggesting that same $Fe(II)_{SORBED}$ redox active pool that did not contribute to the XAS signal (Figure 2,B) participated in Cr(VI) reduction. Lastly, although Cr(VI) reduction was significantly enhanced by $Fe(II)_{SORBED}$, the kinetics were considerably slower, by a factor of about 5000, compared to homogeneous reduction by the equivalent aqueous Fe(II). Examination of homogeneous reduction product by FIB-TEM (Figure S8) revealed amorphous nanometer-sized Cr(III)-Fe(III) rich particles that from XAS analysis contain goethite-like Fe *L*-edge, Cr *L*-edge, and O *K*-edge features (Figure S9).

DISCUSSION

Removal of redox active contaminants in solution (in the absence of solubility-controlling solids) proceeds via two major pathways: i) adsorption into mineral surfaces; and ii) reduction reactions.

335 Specific to this study, removal of oxyanions by adsorption would be an essential pathway if
336 mineral surface complexation sites are positively charged. At the experimental pH ~ 8.6 the
337 positively charged sites in montmorillonite and kaolinite minerals, that dominate the <2 μm clay
338 fraction (Table S7), would be absent or minimal resulting in negligible chromate adsorption.[18,66]
339 We further discuss the removal of oxyanions by reduction pathway.

340 **Identification of reactive mineral phases for Tc(VII) and Cr(VI) reduction**

341 *Effect of minor Fe-sulfide component.* The coexistence of very small quantities of Fe-
342 sulfides, with the ferruginous montmorillonite, raises the question as to whether sulfides
343 contribute to Tc(VII) and/or Cr(VI) reduction at the experimental pH.[20,67-72] In fact, at pH values
344 ranging from 5 to 8, slow Cr(VI) reduction kinetics are linked to pyrite while fast kinetics are
345 linked to metastable mackinawite.[68] Both solid phases possibly are present in the RTZ anoxic
346 clay fraction (Figure S2). Another work[20] with mixed mineral phases including ferruginous
347 smectite, identified pyrite as the most reactive Fe(II)-bearing mineral for Tc(VII) reduction, even
348 though pyrite was a minor component. Yet the present study reveals no correlation between
349 contaminant reduction products and Fe-sulfide particulates (Figure 3b). Presumably, the first
350 step in the oxidation of Fe-sulfides at circumneutral pH is the adsorption of oxidant molecules
351 from solution onto the mineral surface.[68,73,74] Redox reactions could be inhibited if surface
352 coatings restrict diffusion and bonding of soluble oxidant moieties.[75,76] Elemental SEM-EDS
353 mapping shows Fe-sulfide particles nearly encapsulated within clay aggregates (Figure 3,b;
354 Supplemental Information Figure S2); non-reactivity therefore could be due to lack of immediate
355 interaction between oxyanions, Tc(VII) and Cr(VI), and Fe-sulfide surfaces.[76,77]

356 *Reduction of Tc(VII) and Cr(VI) by ferruginous montmorillonite.* Ferruginous
357 montmorillonite, with its considerable natively reduced state of $Fe(II)/Fe_{TOTAL} \sim 0.23$, is the
358 primary Fe(II) bearing mineral and evidently the most redox reactive phase in the RTZ anoxic
359 clay fraction. However, it displays insignificant redox reactivity with Tc(VII) and only partially
360 reduces Cr(VI) (Figure 1,a-c). The difference in reactivity with Tc(VII) compared to Cr(VI) is
361 likely related to the difference in redox potential between Cr(VI)/Cr(III) ($E^o = 1.51V$) and
362 Tc(VII)/Tc(III) ($E^o=0.746$ V).[78] Given the reduction results, we deduce that the redox potential
363 of the naturally anoxic clay is within these bounds ($0.746 < E^o_{RTZanoxic} < 1.51$). Furthermore,
364 based on maximum reduction observed in 50 μM Cr(VI) experiment (Figure 1,c) we estimate
365 the redox capacity of the anoxic clay in its pristine state to be ~ 3.3 μmol reducing-equivalents/g
366 clay. This value is significantly lower than the expected 45 μmol reducing-equivalents/g clay
367 based on 0.5 M HCl extraction of $Fe(II)_{LABILE}$ (Table 1). It suggests that except for Fe(II) in the
368 outermost clay surface (Figure 2,A), the majority of $Fe(II)_{LABILE}$ does not participate in redox
369 reactions.

370 These combined results demonstrate that native anoxic clay displays considerably lower
371 redox reactivity than would be projected from studies with biologically or chemically reduced
372 analogs.[27,33-36,79,80] In such studies, model clays typically have undergone a single reduction
373 event, except for one study wherein two cycles of bioreduction/reoxidation were applied to a
374 model clay[49], that likely resulted in a surplus of surface-bound Fe(II) in newly transformed
375 mineral phases accelerating clay redox kinetics.[33,80-82] In contrast, numerous redox cycles
376 required to fully equilibrate structural Fe(II) content, can result in clay structural changes that
377 decrease its redox reactivity.[50] In the case of the RTZ stratum, it is reasonable to assume that
378 clay minerals have been subjected to several redox cycles arising from seasonal water table

fluctuations, resulting in slow transformation to an Fe-clay containing more stable and less reactive structural Fe(II).

Fe(II) retention by RTZ anoxic clay. Fe(II) sorption by RTZ anoxic clay is characterized by fast kinetics and strong retention. Competitive desorption experiments show no release of aqueous Fe(II) from clay edge or basal/interlayer sites, suggesting that Fe(II) sorption is irreversible (Table 2). Observed irreversibility can perhaps be linked to heterogeneous oxidation/precipitation reactions, i.e., formation of $Fe(OH)_2(s)$ despite undersaturation; or oxidation of Fe(II) to Fe(III) by trace O_2 despite rigorous anoxic conditions followed by $Fe(OH)_3(s)$ precipitation. However, comparison of acid extractions at pH ~4 before and after Fe(II) sorption (Table S7) reveals only minor differences in Fe(II) or Fe(III) concentration. Furthermore, the absence of iron hydroxide precipitates is corroborated by Fe *L*-edge XAS data that show no alteration in clay Fe valence or site symmetry after Fe(II) uptake (Figure 2,B). Another hypothesis for sorption irreversibility could be related to Fe(II) adsorption-induced interfacial ET reactions, from highly reactive surface-bound Fe(II) to clay structural Fe(III).[42,44,45,83] We suggested previously that Fe(II) initially adsorbs to clay edge sites, a suggestion corroborated by density functional theory (DFT) calculations, which demonstrate that edge sites are most energetically favorable for adsorption of Fe(II) in nontronite, particularly if the sites are Fe-O(H) terminated.[48] Presumably, these termination sites are available in the RTZ clay, based on Fe substitution for Al in the clay octahedral sheet (Table 1). DFT calculations further predict that interfacial ET reactions proceed predominantly through the resulting Fe(II)-Fe(III)-O[48] edge surface complexes and, albeit to a much lesser extent, ET contributions from Fe(II) in basal/interlayer sites across tetrahedral sheets have not been ruled out.[44,81] Based on our observations, including Fe *L*-edge XAS data showing that the anoxic clay oxidation state remains

unchanged at near surface after Fe(II) uptake, we hypothesize that added Fe(II) sorbs in a form that is not preserved as redox reactive species at the outermost clay surface, due to sorption-induced ET reactions.

Linking Fe(II) retention to contaminant reduction.

Natural anoxic clay that contains 45 μmol/g $Fe(II)_{LABILE}$, exhibits a finite reduction capacity for Tc(VII) and Cr(VI) that is only marginally increased by Fe(II) uptake (if $Fe(II)_{SORBED}$ is up to 8% of $Fe(II)_{LABILE}$) (Figure 1). However, if Fe(II) added constitutes ~37% of $Fe(II)_{LABILE}$, the extent of Cr(VI) reduction is enhanced significantly. Despite that $FeCl_2$ addition decreased the experimental pH, from pH 8.6 to 7.3 (Table 2), we argue that removal of Cr(VI) from solution was due to reduction and not due to enhancement in chromate adsorption at the lower pH. In fact, Cr(VI) adsorption on smectite is negligible above pH 6.5[18]. Meanwhile adsorption by kaolinite at circumneutral pH 7 varies between 5 to 10%[18,66] contingent on kaolinite pre-treatment and on solid to Cr(VI) ratio. In either case these values that cannot account for Cr(VI) removal from solution as indicated in Figure 1,f.

The observation that Fe(II) is non-exchangeable after sorption suggests that reduction of Cr(VI) is surface mediated. This assumption at first seems contradictory considering the presence of micron-sized discrete Cr-Fe particles, which could indicate homogeneous Cr(VI) reduction by Fe(II) exchanged in solution.[26] However the appearance of isolated Cr-Fe particles as nanometer-sized crystallites contrasts the amorphous nature of precipitates formed homogeneously (Figure S6-S9) implying that reduction of Cr(VI) was mediated at localized sites, near or at the clay surface. We further speculate that the Cr-Fe nano-crystallites likely aggregated into larger particles during centrifugation, due to their higher solid density. This

reasoning is based on two observations i) absence of Cr-Fe discrete particles in non-centrifuged samples; and ii) a significant increase in clay matrix aggregation after centrifugation (Figure S10). Further, the difference between Cr-Fe crystallites in the heterogeneous system and the amorphous Cr(III)-Fe(III) precipitate in the homogenous system (Figure S7, S8) supports the surface-mediated mechanism.

Lastly, reduction of Cr(VI) by sorbed Fe(II) is slow, compared to literature-based precedent.[40] The slow kinetics arguably could be related to Coulombic repulsion forces between the oxyanions, Tc(VII) and Cr(VI), and the negatively charged clay surface at slightly basic pH. Additionally, slow kinetics could be indicative of the sluggishness of extracting electron equivalents retained within clay interiors. Our analyses provide clear evidence that although surplus Fe(II) is not present as redox reactive species within the outermost few nanometers of clay surfaces likely due to ET, the reducing equivalents remain stored in the clay interiors. Addition of a strong oxidant in solution is a test of the ET reversibility of the resulting system and emphasizes a significant contrast between fast kinetics of electron uptake and sluggish kinetics of electron release by the native anoxic clay. The slow reduction kinetics thus may arise from diffusion-limited rates of electron hopping from the inner surface of clay minerals back to edge, or perhaps basal, sites where weakly interacting oxyanions can accept electrons. The findings here improve our understandings of RTZ's geochemical redox kinetics with Tc(VII) and Cr(VI), which lead to better predict the mobility of single or multiple contaminants that infiltrate subsurface sediments and compete for available electrons in naturally reduced zones.[84,85] The presence of clay minerals, with large sorption capacities in sediment composites, effects Fe(II) adsorption and leads to ET reactions within clay mineral that can renew the natural redox boundaries in poorly drained sediments and soils.[86] . We showed that in fact only a small

447 increase, between 0.4 to 5.6% of added/sorbed Fe(II) (over $Fe(II)_{STRUCTURAL}$) renewed the redox
448 capacity of anoxic clay fraction with respect to chromate reduction. This type of redox capacity
449 recharging by adsorbed Fe(II) is of particular significance in mitigating contaminant transport in
450 systems with low total organic carbon or in environments deficient in bacterial colonies.[86]

451 **ENVIRONMENTAL IMPLICATIONS**

452 The present study examines reduction of oxyanions, Tc(VII) and Cr(VI), by the anoxic clay
453 fraction of a fine-grained sediment from an RTZ that is dominated mineralogically by a naturally
454 reduced ferruginous montmorillonite. In doing so it fills an important knowledge gap pertaining
455 to the real-world applicability of the many laboratory studies on model Fe-clay isolates
456 motivated to understand natural system behavior. Minor amounts of Fe-sulfide that coexist in
457 clay fraction appear not to participate in redox reactions likely because they are encapsulated
458 within clay particles. Contaminant reduction kinetics, by the ferruginous montmorillonite at its
459 native pH of 8.6, are sluggish, despite the significant reduced state of clay mineral
460 ($Fe(II)/Fe_{TOTAL} \sim 0.23$) and expectations derived from model system studies. Reduction rate and
461 extent are enhanced by sorption of aqueous Fe(II), if the concentration of $Fe(II)_{SORBED}$ surpasses
462 the finite reduction capacity of the native clay. Probable redox pathways, upon exposure to
463 aqueous Fe(II) and then to redox active contaminants, appear to include: i) fast sorption induced
464 ET from $Fe(II)_{SORBED}$ to $Fe(III)_{STRUCTURAL}$; and ii) slow reverse ET induced by addition of a
465 strong redox but weakly adsorbed species in solution e.g. Cr(VI), resulting in contaminant
466 reduction.

467 For the Hanford site in particular, this study builds on previous RTZ work performed on the
468 hosting coarser fraction[20] and its partner whole sediment[52] from a nearby location, by reinforcing

that faster Tc(VII) reduction kinetics reported therein are solely due to the contributions of other Fe(II)-rich minerals (siderite/pyrite) and not of Fe(II)-rich smectite. Present study establishes that the redox capacity of the clay component is significantly lower than that expected from studies with reduced model clays. This raises important issues regarding contaminant mobility in analogous sites that undergo numerous redox fluctuations, including the accuracy of contaminant retardation predictions based on laboratory studies of model systems that are chemically or biologically reduced in limited redox cycles.[27,33-36,49,79,80]

ACKNOWLEDGEMENTS

This work is based upon research supported by the U.S. Department of Energy (DOE) Office of Science, Office of Biological and Environmental Research (OBER), through its Subsurface Biogeochemical Research (SBR) Science Focus Area (SFA) program at Pacific Northwest National Laboratory. Microscopic analyses were performed in the William R. Wiley Environmental Molecular Science Laboratory (EMSL), a national user facility supported by the OBER and located at PNNL. XAS and XMCD measurements were performed at the Advance Light Source supported by the DOE Office of Science, Office of Basic Energy Sciences under Contract No. DE-AC02-05CH11231. We thank Drew Latta (University of Iowa) for Mössbauer measurements.

ASSOCIATED CONTENT

Supporting Information

Description of analytical methods, which include sediment separation, total digestion, elemental analysis, XRD, microscopy, and EXAFS/XAS/Mössbauer spectroscopy and spectra analysis. Tables show sediment mineralogy, clay redox capacity, Mössbauer spectral fitting,

491 EXAFS /LCF fitting, and sediment acid extraction. Figures show pre-reaction XRD data, SEM
492 mapping of anoxic clay, EXAFS, and Mössbauer spectra; post-reaction XAS data, TEM
493 diffraction patterns of heterogeneous/homogeneous Cr-Fe reaction product, SEM micrographs of
494 clay aggregates.

495 **AUTHOR INFORMATION**

496 Corresponding Author

497 *E-mail: odeta.qafoku@pnnl.gov. Tel: 509-371-6383

498

499

500

501

502

503

504

505

506

507

508

509 **Table 1:** Chemical analysis of < 2µm clay fractions of Hanford sediments collected from
510 RTZ oxic and anoxic interface. Both horizons have same total Fe content, yet differ significantly
511 by Fe(II) concentration. Calculated clay unit formula reveals that Fe and Mg substituted for Al
512 in the octahedral sheet.

RTZ Horizon	SA (m^2/g)	Inorganic C (%)	CEC (meq/g)	Exchangable cations (mmol/g)				[a]Fe_{dig} speciation (mmol/g)		[b]$Fe(II)_{HCl}$ (mmol/g)	[c]Fe_{ca} (mmol/g)
				Ca^{2+}	Mg^{2+}	Na^{+}	K^{+}	Fe(II)	Fe(III)		
[d]Oxidized 18 – 18.3 m	141.8	< 0.02	0.811	0.261	0.08	0.027	0.016	0.062	1.281	n.a.	0.005
Reduced 18.6 – 18.9 m	104.7	0.0238	0.862	0.239	0.081	0.021	0.023	0.298	1.032	0.045	0.011

513

514

515

516

517

518

519 [a]Fe digestion

520 [b]1h 0.5M HCl extractable Fe(II)

521 [c]citrate/ascorbate extractable Fe

522 [d]Approximate structural formula for clay mineral after complete digestion of clay fraction in HF/H_2SO_4
523 mixture The minor phase impurities identified by XRD (Figure S1) were taken into account prior to unit
524 formula calculation.

525 Oxidized Clay: $Ca_{0.28}\ K_{0.29}Mg_{0.08}Na_{0.03}\ (Al_{2.17}Fe^{3+}_{1.21}Fe^{2+}_{0.06}Mg_{0.61})(Si_{7.36}Ti_{0.09}Al_{0.55})O_{20}(OH)_4$

526 Reduced Clay: $Ca_{0.29}\ K_{0.29}Mg_{0.07}Na_{0.09}(Al_{2.34}Fe^{3+}_{0.87}Fe^{2+}_{0.25}Mg_{0.60})(Si_{7.43}Ti_{0.12}Al_{0.45})O_{20}(OH)_4$

Figure 1: Tc(VII) and Cr(VI) reduction over time (~50d) by native (a,b,c) and Fe(II) (10µ and 150µM) amended anoxic clay fraction. Panels a,d show reduction kinetics of 2.5µM Tc(VII). Panels b,e and c,f respectively, show reduction kinetics of 2.5 µM and 50 µM Cr(VI). Equilibration pH varied between 8.7-8.9 for native anoxic clay fraction and between 7.6-8.0 for Fe(II)-amended anoxic clay fraction.

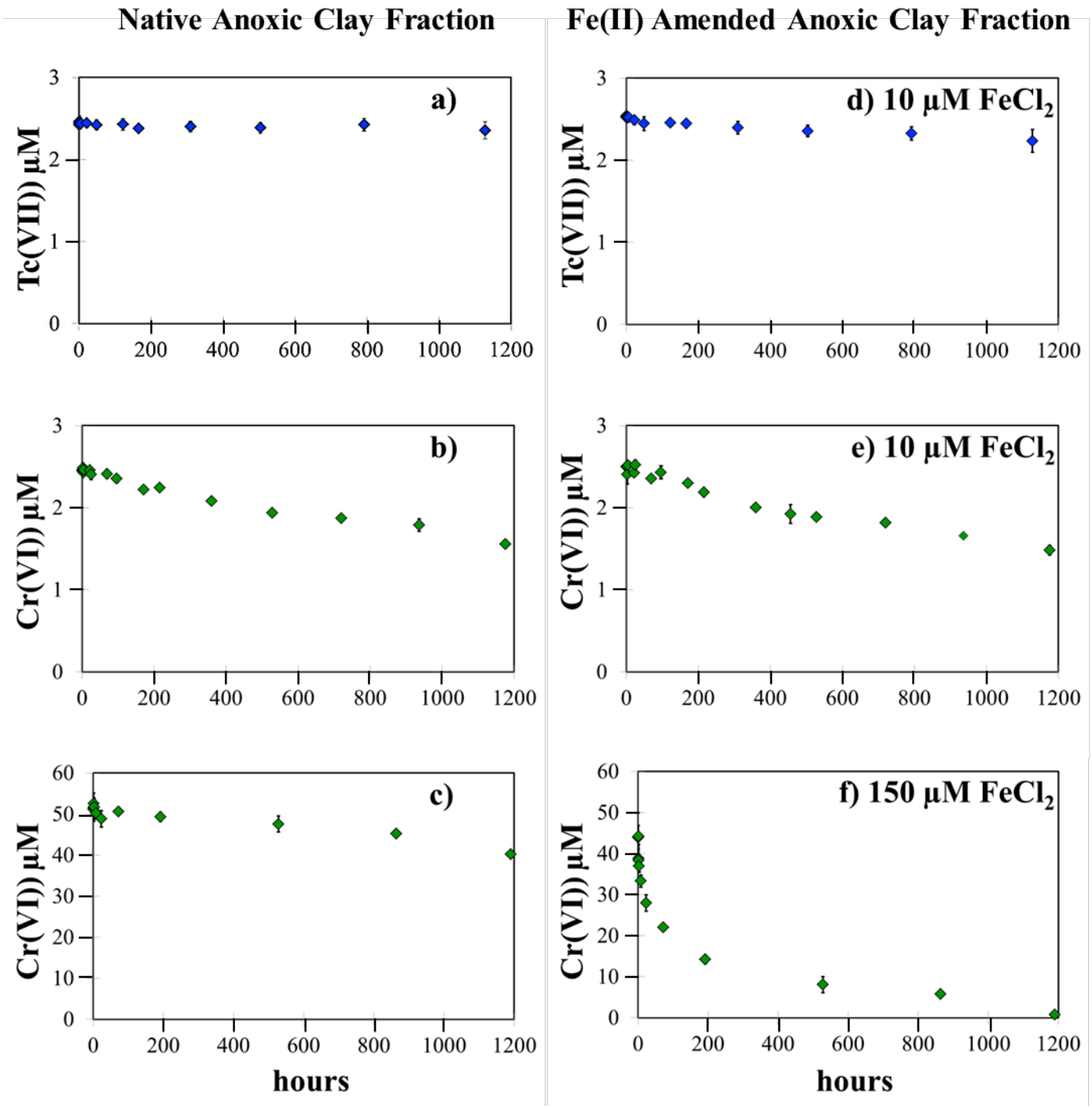

A

B

Figure 2: A. XAS spectra of native anoxic clay before reaction (black line) and post reaction with 50µM Cr(VI) (red line), show a decrease in peak intensity on the low energy side of the Fe L_3 spectrum after reaction. B. XAS spectra of anoxic clay before and after exposure to 150 µM Fe(II) shows no signal change in the XAS spectra (detection limit 1- 2%). C. XAS spectra of reduced Hanford clay exposed to Fe(II) before and after reaction with 50 µM Cr(VI) (no signal change was observed in the XAS spectra despite the significant Cr(VI) removal.)

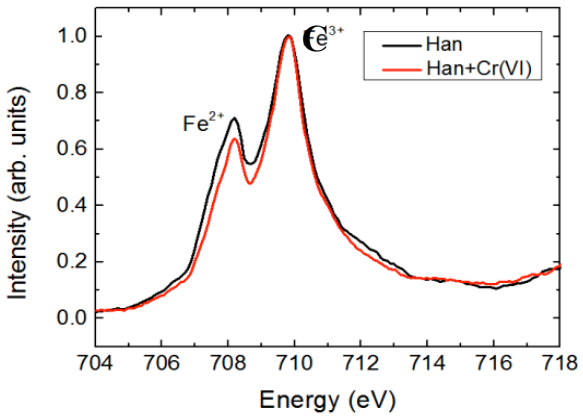

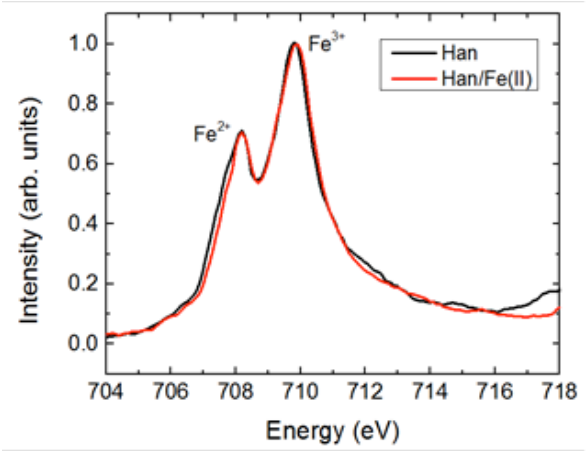

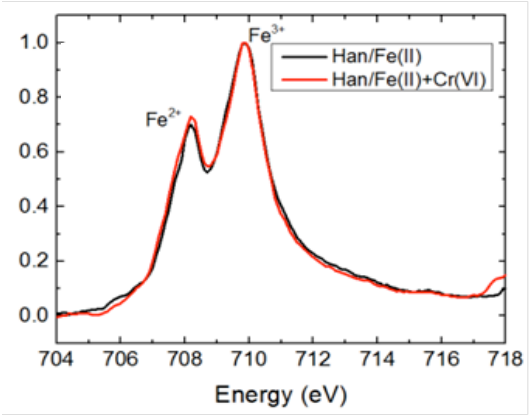

Table 2: 150µM Fe(II) sorption is associated with release of exchangeable cations (Mg^{2+}, K^{+}, Ca^{2+}) from clay interlayer sites. Competitive desorption experiments (Column 6-8) show no release of sorbed Fe(II) from clay sites, suggesting that Fe(II) sorption is irreversible.

Hanford Anoxic Clay	Suspension density: 9g/L				24h extractions post 150µM Fe^{2+} sorption[c,d]			
	Deionized H_2O	10µM Fe^{2+}, ½ h equilibration	150µM Fe^{2+}, ½ h equilibration	150µM HCl, ½ h equilibration[a]	10mM $MgCl_2$	100mM $CaCl_2$	1M NH_4Acetate pH 7	1M NaH_2PO_4 pH 5
Suspension pH	8.6	8.5	7.3	7.2	n/a	n/a	n/a	n/a
Fe^{2+} (µmol/g)	b.d.[b]	0.03± 0.04	0.20± 0.13	0.05± 0.02	0.00	0.33± 0.06	0.00	b.d.[e]
Total Fe (µmol/g)	0.67± 0.04	0.73± 0.12	0.97± 0.31	0.81± 0.23	0.31± 0.13	0.70± 0.03	0.31± 0.10	n/a
$_{aq}Mg^{2+}$(µmol/g)	2.31± 0.12	2.48± 0.10	7.48± 0.29	4.90± 0.31	n/a[e]	97.7± 2.94	84.3± 5.63	n/a
$_{aq}Ca^{2+}$(µmol/g)$^{+}$	5.76± 0.14	5.89± 0.28	18.8± 0.96	12.3± 0.36	199.7± 12.4	n.a.	257.6± 25.0	n/a
$_{aq}K^{++}$(µmol/g)	6.66± 0.02	7.05± 0.08	9.81± 1.53	7.46± 0.36	18.8± 0.9	33.2± 1.42	54.8± 10.9	n/a
$_{aq}Na^{++}$(µmol/g)	5.10± 0.05	5.30± 0.09	5.56± 0.96	6.17± 0.37	12.4± 1.6	22.5± 1.94	10.7± 1.13	n/a

[a]0.150 mM Fe^{2+} control experiments showed no oxidation of Fe^{2+} during the course of experiment; [b]. b.d. below detection with ferrozine method.; [c]. further extractions in 10mM NaCl, 1M $CaCl_2$, and 1M $MgCl_2$, showed no release of Fe^{2+} after 24h equilibration.; [d.] Fe^{2+} release in 1M NaH_2PO_4 was monitored at 18hours of equilibration, [e]. at pH 5, the solution phase of 150µM Fe^{2+} and 1M PO_4^{3-}, is undersaturated with respect to vivianite [f]. n/a non available.

Figure 3: 50 µM Cr(VI) post-reaction SEM-EDS compositional mappings of anoxic clay fraction amended with 150 µM Fe(II). Micrographs show high Z-contrast discrete particles rich in Cr and Fe (a,b) that were not found in natural anoxic clay fraction. Cr-Fe rich particles have irregular shapes and non-specific morphology. No association was found between Cr and Fe-sulfide particles after analyzing sixteen FeS_x particulates. Clay minerals are depicted by light grey background.

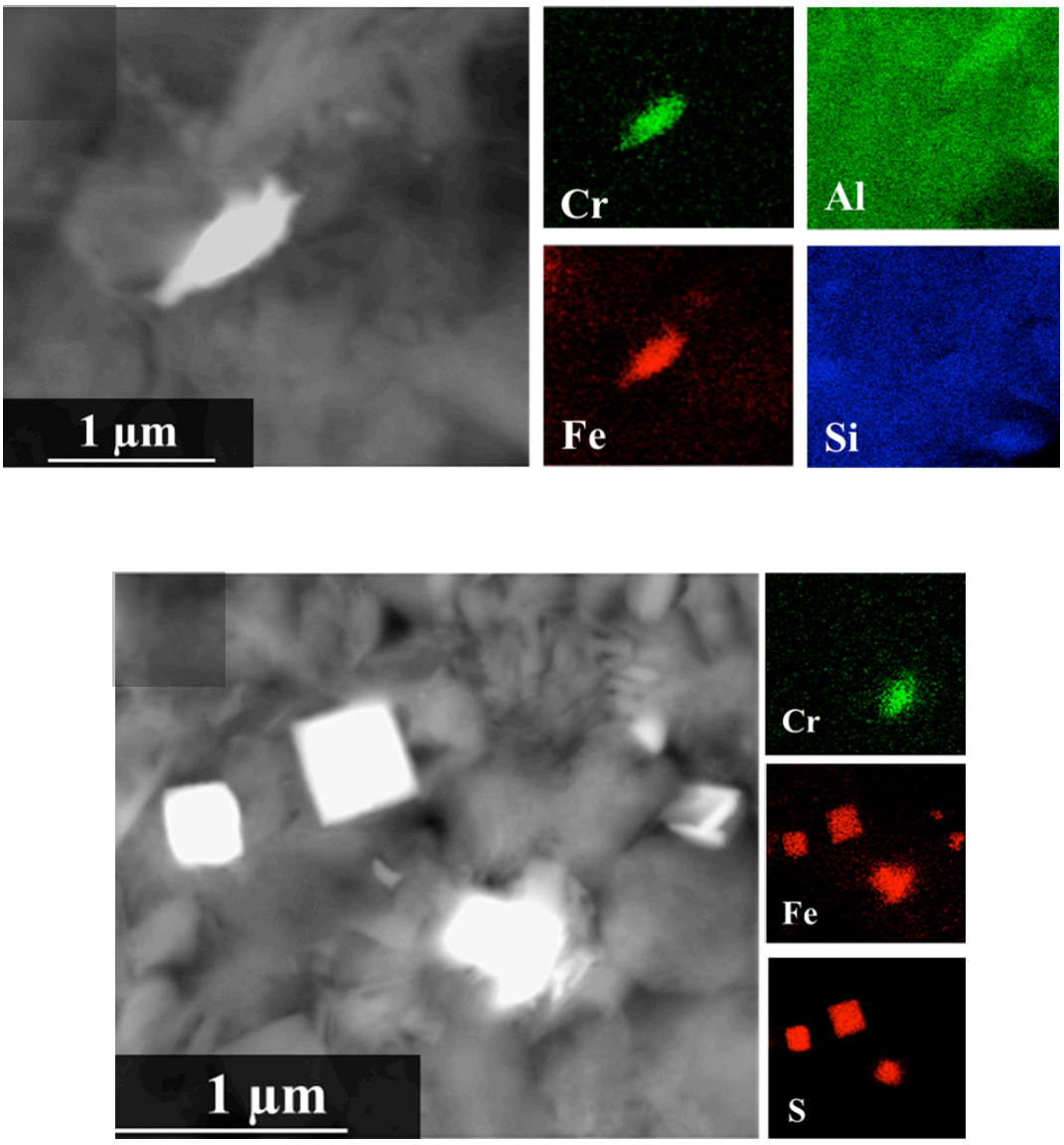

References

1. Stucki, J.W.; Komadel, P.; Wilkinson, H.T. Microbial Reduction of Structural Iron(III) in Smectites. *Soil Sci. Soc. Am. J.* **1987**, 51, 1663-1665.
2. Gates, W.P.; Wilkinson, H.T.; Stucki, J.W. Swelling Properties of Microbially Reduced Ferruginous Smectite. *Clays Clay Miner.***1993**, 41, 360-364.
3. Kostka, J.E.; Stucki, J.W.; Nealson, K.H.; Wu, J. Reduction of structural Fe(III) in smectite by a pure culture of Shewanella putrefaciens strain MR-1. *Clays Clay Miner.* **1996**, 44, 522-529.
4. Ernstsen, V.; Gates, W.P.; Stucki, J.W. Microbial reduction of structural iron in clays - A renewable source of reduction capacity. *J. Environ. Qual.* **1998**, 27, 761-766.
5. Hofstetter, T.B.; Schwarzenbach, R.P.; Haderlein, S.B. Reactivity of Fe(II) species associated with clay minerals. *Environ. Sci. Technol.* **2003**, 37, 519-528.
6. Neumann, A.; Hofstetter, T.B.; Lussi, M.; Cirpka, O.A.; Petit, S.; Schwarzenbach, R.P. Assessing the Redox Reactivity of Structural Iron in Smectites Using Nitroaromatic Compounds As Kinetic Probes. *Environ. Sci. Technol.* **2008**, 42, 8381-8387.
7. Brigatti, M.F.; Franchini, G.; Lugli, C.; Medici, L.; Poppi, L.; Turci, E. Interaction between aqueous chromium solutions and layer silicates. *Appl. Geochem.* **2000**, 15, 1307-1316.
8. Brigatti, M.F.; Lugli, C.; Cibin, G.; Marcelli, A.; Giuli, G.; Paris, E.; Mottana, A.; Wu, Z.Y. Reduction and sorption of chromium by Fe(II)-bearing phyllosilicates: Chemical treatments and X-ray absorption spectroscopy (XAS) studies. *Clays Clay Miner.* **2000**, 48, 272-281.
9. Ilton, E.S.; Haiduc, A.; Moses, C.O.; Heald, S.M.; Elbert, D.C.; Veblen, D.R. Heterogeneous reduction of uranyl by micas: Crystal chemical and solution controls. *Geochim. Cosmochim. Ac.* **2004**, 68, 2417-2435.
10. Ilton, E.S.; Veblen, D.R. Chromium sorption by phlogopite and biotite in acidic solutins at 25 °C – Insights from X-ray Photoelectron-Spectroscopy and Electron-Microscopy. *Geochim Cosmochim. Ac.* **1994**, 58, 2777-2788.
11. Ilton, E.S.; Veblen, D.R., Moses, C.O.; Raeburn, S.P. The catalytic effect of sodium and lithium ions on coupled sorption-reduction of chromate at the biotite edge-fluid interface. *Geochim Cosmochim. Ac.* **1997**, 61, 3543-3563.
12. Schroeder, N.C.; Morgan, D.; Rokop, D.J.; Fabrykamartin, J. Migration of Tc-99 in the Alluvial Aquifer at the Nevada Test Site, Nevada. *Radiochim. Acta.* **1993**, 60, 203-209.
13. Wildung, R.E.; Mcfadden, K.M.; Garland, T.R. Technetium Sources and Behavior in the Environment. *J. Environ. Qual.* **1979**, 8, 156-161.
14. Fruchter, J.S.; Cole, C.R.; Williams, M.D.; Vermeul, V.R.; Amonette, J.E.; Szecsody, J.E.; Istok, J.D.; Humphrey, M.D. Creation of a subsurface permeable treatment zone for aqueous chromate contamination using in situ redox manipulation. *Ground Water Monit. R.* **2000**, 20, 66-77.
15. Zachara, J.M.; Ainsworth, C.C.; Brown, G.E.; Catalano, J.G.; McKinley, J.P.; Qafoku, O.; Smith, S.C.; Szecsody, J.E.; Traina, S.J.; Warner, J.A. Chromium speciation and mobility in a high level nuclear waste vadose zone plume. *Geochim. Cosmochim. Ac.* **2004**, 68, 13-30.
16. Qafoku, N.P.; Ainsworth, C.C.; Szecsody, J.E.; Qafoku, O.S.; Heald, S.M. Effect of coupled dissolution and redox reactions on Cr(VI)(aq) attenuation during transport in the sediments under hyperalkaline conditions. *Environ. Sci. Technol.* **2003**, 37, 3640-3646

17. Qafoku, N.P.; Dresel, P.E.; McKinley, J.P.; Liu, C.X.; Heald, S.M.; Ainsworth, C.C.; Phillips, J.L.; Fruchter, J.S. Pathways of Aqueous Cr(VI) Attenuation in a Slightly Alkaline Oxic Subsurface. *Environ. Sci. Technol.* **2009**, 43, 1071-1077.
18. Rai, D.; Eary, L.E.; Zachara, J.M. Environmental Chemistry of Chromium. *Sci Total Environ.* **1989**, 86, 15-23.
19. Zachara, J.M.; Heald, S.M.; Jeon, B.H.; Kukkadapu, R.K.; Liu, C.X.; McKinley, J.P.; Dohnalkova, A.C.; Moore, D.A. Reduction of pertechnetate [Tc(VII)] by aqueous Fe(II) and the nature of solid phase redox products. *Geochim. Cosmochim. Ac.* **2007**, 71, 2137-2157.
20. Peretyazhko, T.S.; Zachara, J.M.; Kukkadapu, R.K.; Heald, S.M.; Kutnyakov, I.V.; Resch, C.T.; Arey, B.W.; Wang, C.M.; Kovarik, L.; Phillips, J.L.; Moore, D.A. Pertechnetate (TcO_4^-) reduction by reactive ferrous iron forms in naturally anoxic, redox transition zone sediments from the Hanford Site, USA. *Geochim. Cosmochim. Ac.* **2012**, 92, 48-66.
21. Cui, D.Q.; Eriksen, T.E. Reduction of pertechnetate in solution by heterogeneous electron transfer from Fe(II)-containing geological material. *Environ. Sci. Technol.* **1996**, 30, 2263-2269.
22. Buerge, I.J.; Hug, S.J. Kinetics and pH dependence of chromium(VI) reduction by iron(II). *Environ. Sci. Technol.* **1997**, 31, 1426-1432.
23. Eary, L.E.; Rai, D. Chromate Removal from Aqueous Wastes by Reduction with Ferrous Ion. *Environ. Sci. Technol.* **1988**, 22, 972-977.
24. Fendorf, S.E.; Li, G.C. Kinetics of chromate reduction by ferrous iron. *Environ. Sci. Technol.* **1996**, 30, 1614-1617.
25. Sedlak, D.L.; Chan, P.G. Reduction of hexavalent chromium by ferrous iron. *Geochim. Cosmochim. Ac.* **1997**, 61, 2185-2192.
26. Eary, L.E.; Rai, D. Kinetics of Chromate Reduction by Ferrous-Ions Derived from Hematite and Biotite at 25-Degrees-C. *Am. J. Sci.* **1989**, 289, 180-213.
27. Bishop, M.E.; Glasser, P.; Dong, H.L.; Arey, B.; Kovarik, L. Reduction and immobilization of hexavalent chromium by microbially reduced Fe-bearing clay minerals. *Geochim. Cosmochim. Ac*. **2014**, 133, 186-203.
28. Taylor, R.W.; Shen, S.Y.; Bleam, W.F.; Tu, S.I. Chromate removal by dithionite-reduced clays: Evidence from direct X-ray adsorption near edge spectroscopy (XANES) of chromate reduction at clay surfaces. *Clays Clay Miner.* **2000**, 48, 648-654.
29. Gan, H.; Bailey, G.W; Shane, Y. Morphology of lead(II) and chromium(III) reaction products on phyllosilicate surfaces as determined by atomic force microscopy. *Clays Clay Miner.* **1996**, 44, 734-743.
30. Hofstetter, T.B.; Neumann, A.;Schwarzenbach, R.P. Reduction of nitroaromatic compounds by Fe(II) species associated with iron-rich smectites. *Environ. Sci. Technol.* **2006**, 40, 235-242.
31. Peterson, M.L.; Brown, G.E.; Parks, G.A. Direct XAFS evidence for heterogeneous redox reaction at the aqueous chromium/magnetite interface. *Colloid Surf. A* **1996**, 107, 77-88.
32. Kendelewicz, T.; Liu, P.; Doyle, C.S.; Brown, G.E. Spectroscopic study of the reaction of aqueous Cr(VI) with Fe_3O_4(111) surfaces. *Surf Sci.* **2000**, 469, 144-163.

33. Bishop, M.E.; Dong, H.L.; Kukkadapu, R.K.; Liu, C.X.; Edelmann, R.E. Bioreduction of Fe-bearing clay minerals and their reactivity toward pertechnetate (Tc-99). *Geochim Cosmochim Ac.* **2011**, 75, 5229-5246.
34. Jaisi, D.P.; Liu, C.X.; Dong, H.L.; Blake, R.E.; Fein, J.B. Fe^{2+} sorption onto nontronite (NAu-2). *Geochim. Cosmochim. Ac.* **2008**, 72, 5361-5371.
35. Jaisi, D.P.; Dong, H.L.; Plymale, A.E.; Fredrickson, J.K.; Zachara, J.M.; Heald, S.; Liu, C.X. Reduction and long-term immobilization of technetium by Fe(II) associated with clay mineral nontronite. *Chem. Geol.* **2009**, 264, 127-138.
36. Peretyazhko, T.; Zachara, J.M.; Heald, S.M.; Jeon, B.H.,;Kukkadapu, R.K.; Liu, C.; Moore, D.; Resch, C.T. Heterogeneous reduction of Tc(VII) by Fe(II) at the solid-water interface. *Geochim. Cosmochim. Ac.* **2008**, 72, 1521-1539.
37. Peretyazhko, T.; Zachara, J.M.; Heald, S.M.; Kukkadapu, R.K.; Liu, C.; Plymale, A.E.; Resch, C.T. Reduction of Tc(VII) by Fe(II) sorbed on Al (hydr)oxides. *Environ. Sci. Technol.* **2008**, 42, 5499-5506.
38. Lovley, D.R. Dissimilatory Metal Reduction. *Annu Rev Microbiol.* **1993**, 47, 263-290.
39. Zachara, J.M.; Fredrickson, J.K.; Li, S.M.; Kennedy, D.W.; Smith, S.C.;Gassman, P.L. Bacterial reduction of crystalline Fe^{3+} oxides in single phase suspensions and subsurface materials. *Am. Mineral.* **1998**, 83, 1426-1443.
40. Buerge, I.J.; Hug, S.J. Influence of mineral surfaces on Chromium(VI) reduction by Iron(II). *Environ. Sci. Technol.* **1999**, 33, 4285-4291.
41. Elsner, M., Schwarzenbach, R.P. and Haderlein, S.B. Reactivity of Fe(II)-bearing minerals toward reductive transformation of organic contaminants. *Environ. Sci. Technol*. **2004**, 38, 799-807.
42. Gehin, A.; Greneche, J.M.; Tournassat, C.; Charlet, L. Specific sorption of Fe(II) on synthetic montmorillonite in anoxic conditions. *Geochim. Cosmochim. Ac.* **2004**, 68, A164-A164.
43. Charlet, L.; Silvester, E.; Liger, E. N-compound reduction and actinide immobilization in surficial fluids by Fe(II): the surface $\equiv Fe^{III}OFe^{II}OH$ degrees species, as major reductant. *Chem. Geol.* 1998, 151, 85-93.
44. Neumann, A.; Olson, T.L.; Scherer, M.M. Spectroscopic Evidence for Fe(II)-Fe(III) Electron Transfer at Clay Mineral Edge and Basal Sites. *Environ. Sci. Technol.* **2013**, 47, 6969-6977.
45. Soltermann, D.; Fernandes, M.M.; Baeyens, B.; Dahn, R.; Joshi, P.A.; Scheinost, A.C.; Gorski, C.A. Fe(II) Uptake on Natural Montmorillonites. I. Macroscopic and Spectroscopic Characterization. *Environ. Sci.Technol.* **2014**, 48, 8688-8697.
46. Schaefer, M.V.; Gorski, C.A.; Scherer, M.M. Spectroscopic Evidence for Interfacial Fe(II) — Fe(III) Electron Transfer in a Clay Mineral. *Environ. Sci.Technol.* **2011**, 45, 540-545.
47. Alexandrov, V.; Neumann, A.; Scherer M.M.; Rosso, K.M. Electron exchange and conduction in nontronite from first-principles. *J. Phys. Chem. C*, **2013**, 117, 2032-2040.
48. Alexandrov, V.; Rosso, K.M. Insights into the mechanism of Fe(II) adsorption and oxidation at Fe-Clay mineral surfaces from first-principles calculations. *J. Phys. Chem. C*, **2013** 117, 22880-22886.
49. Yang, J.J.; Kukkadapu, R.K.; Dong, H.L.; Shelobolina, E.S.; Zhang, J.; Kim, J. Effects of redox cycling of iron in nontronite on reduction of technetium. *Chem. Geol.* **2012**, 291, 206-216.

50. Stucki, J.W. A review of the effects of iron redox cycles on smectite properties. *C. R. Geosci.* **2011**, 343, 199-209.
51. Gorski, C. A.; Klüpfel, L. E.; Voegelin, A.; Sander, M.; Hofstetter, T. B., Redox Properties of Structural Fe in Clay Minerals: 3. Relationships between Smectite Redox and Structural Properties. *Environ. Sci. Technol.* **2013,** *47*, (23), 13477-13485.
52. Yan, S.; Liu, Y.; Liu, C.; Shi, L.; Shang, J.; Shan, H.; Zachara, J.M.; Fredrickson J.K.; Kennedy, D.; Resch, C.T.; Thompson, C.; Fansler, S. Nitrate bioreduction in redox-variable low permeability sediments. Sci. Total Environ. 2016, 539, 185-195.
53. Lin, X.J.; Kennedy, D.; Fredrickson, J.; Bjornstad, B.; Konopka, A. Vertical stratification of subsurface microbial community composition across geological formations at the Hanford Site. *Environ. Microbiol.* **2012**, 14, 414-425.
54. Lin, X.J.; Kennedy, D.; Peacock, A.; McKinley, J.; Resch, C.T.; Fredrickson, J.;Konopka, A. Distribution of Microbial Biomass and Potential for Anaerobic Respiration in Hanford Site 300 Area Subsurface Sediment. *Appl. Environ. Microb.* **2012**, 78, 759-767.
55. More, D.M.; Reynolds, R.C.Jr. *X-Ray Diffraction and the Identification and analysis of Clay Minerals.* Oxford University Press: Oxford, U.K., 1997
56. Brunauer, S.; Emmett, P.H.; Teller, E. Adsorption of gases in multimolecular layers. *J. Am. Chem. Soc.* **1938**, 60, 309-319.
57. Amonette , J.E.; Templeton, J.C. Improvements to the quantitative assay of nonrefractory minerals for Fe(II) and total Fe using 1,10-Phenantholine. *Clays Clay Miner.***1998**, 46, 51-62
58. Arenholz, E.;Prestemon, S.O. Design and performance of an eight-pole resistive magnet for soft x-ray magnetic dichroism measurements. *Rev. Sci. Instrum.* **2005**, 76.
59. Stookey, L.L. Ferrozine - a New Spectrophotometric Reagent for Iron. *Anal. Chem*. **1970**, 42, 779-781.
60. Zachara, J.M.; Serne, J.; Freshley, M.; Mann, F.; Anderson, F.; Wood, M.; Jones, T.; Myers, D. Geochemical processes controlling migration of tank wastes in Hanford's vadose zone. *Vadose Zone J.* **2007**, 6, 985-1003.
61. Brindley, G.W; Brown, G. Eds. Crystal Structures of Clay Minerals and their X-ray identification, Mineralogical Society: London, U.K., 1980
62. Stucki, J. W.; Golden, D. C.; Roth, C. B. Preparation and handling of dithionite-reduced smectite suspensions. *Clays Clay Miner.* **1984,** 32, 191−197
63. Dyar, M.D.; Schaefer, M.W.; Sklute, E.C.; Bishop, J.L. Mossbauer spectroscopy of phyllosilicates: effects of fitting models on recoil-free fractions and redox ratios. *Clay Miner.* **2008**, 43, 3-33.
64. Tsarev, S.; Waite, T.D.; Collins, R.N. Uranium Reduction by Fe(II) in the Presence of Montmorillonite and Nontronite. *Environ. Sci. Technol.* **2016**, 50, 8223-8230
65. Schultz, C.; Grundl, T. pH dependence of ferrous sorption onto two smectite clays. *Chemosphere* **2004**, 57, 1301-1306
66. Ward, N.E. Adsorption of Hexavalent Chromium on Koalinite and Illite. Master Dissertation, The University of Arizona, Tucson, AZ, 1990
67. Mullet, M.; Boursiquot, S.; Ehrhardt, J.J. Removal of hexavalent chromium from solutions by mackinawite, tetragonal FeS. *Colloid Surface A* **2004**, 244, 77-85.

68. Patterson, R.R.; Fendorf, S.; Fendorf, M. Reduction of hexavalent chromium by amorphous iron sulfide. *Environ. Sci. Technol.* **1997**, 31, 2039-2044.
69. Demoisson, F.; Mullet, M.; Humbert, B. Pyrite oxidation by hexavalent chromium: Investigation of the chemical processes by monitoring of aqueous metal species. *Environ. Sci. Technol.* **2005**, 39, 8747-8752.
70. Zouboulis, A.I.; Kydros, K.A.; Matis, K.A. Removal of Hexavalent Chromium Anions from Solutions by Pyrite Fines. *Water Res.* **1995**, 29, 1755-1760.
71. Geraedts, K.; Bruggeman, C.; Maes, A.; Van Loon, L.R.; Rossberg, A.; Reich, T. Evidence for the existence of Tc(IV) - humic substance species by X-ray absorption near-edge spectroscopy. *Radiochim. Acta* **2002**, 90, 879-884.
72. Maes, A.; Geraedts, K.; Bruggeman, C.;, Vancluysen, J.; Rossberg, A.; Hennig, C. Evidence for the interaction of technetium colloids with humic substances by X-ray absorption spectroscopy. *Environ. Sci. Technol.* **2004**, 38, 2044-2051.
73. Luther, G.W. Pyrite Oxidation and Reduction - Molecular-Orbital Theory Considerations. *Geochim. Cosmochim. Ac.* **1987**, 51, 3193-3199.
74. Gartman, A. and Luther, G.W. Oxidation of synthesized sub-micron pyrite (FeS2) in seawater. *Geochim. Cosmochim. Ac.* **2014**, 144, 96-108.
75. Nicholson, R.V.; Gillham, R.W.; Reardon, E.J. Pyrite Oxidation in Carbonate-Buffered Solution .1. Experimental Kinetics. *Geochim. Cosmochim. Ac.* **1988**, 52, 1077-1085.
76. Huminicki, D.M.C.; Rimstidt, J.D. Iron oxyhydroxide coating of pyrite for acid mine drainage control. *Appl. Geochem.* **2009**, 24, 1626-1634.
77. Vandiviere, M.M.; Evangelou, V.P. Comparative testing between conventional and microencapsulation approaches in controlling pyrite oxidation. *J. Geochem. Explor.* **1998**,64, 161-176.
78. Rard, J.A.; Rand, M.H.; Anderegg, G.; Wanner, G. *Chemical Thermodynamic of Technetium.* Elsevier: Amsterdam, Holland, 1999,
79. Fredrickson, J.K.; Zachara, J.M.; Kennedy, D.W.; Kukkadapu, R.K.; McKinley, J.P.; Heald, S.M.; Liu, C.X.; Plymale, A.E. Reduction of TcO_4^- by sediment-associated biogenic Fe(II). *Geochim. Cosmochim. Ac*. **2004**, 68, 3171-3187.
80. Fredrickson, J.K.; Zachara, J.M.; Plymale, A.E.; Heald, S.M.; McKinley, J.P.; Kennedy, D.W.; Liu, C.X.; Nachimuthu, P. Oxidative dissolution potential of biogenic and abiogenic TcO_2 in subsurface sediments. *Geochim. Cosmochim. Ac.* **2009**, 73, 2299-2313.
81. Brookshaw, D.R.; Coker, V.S.; Lloyd, J.R.; Vaughan, D.J.; Pattrick, R.A.D. Redox Interactions Between Cr(VI) and Fe(II) in Bioreduced Biotite and Chlorite. *Environ. Sci. Technol*. **2014**, 48, 11337-11342.
82. Brookshaw, D.R.; Pattrick, R.A.D.; Bots, P.; Law, G.T.W.; Lloyd, J.R.; Mosselmans, J.F.W.; Vaughan, D.J.; Dardenne, K.; Morrie, K. Redox Interactions of Tc(VII), U(VI), and Np(V) with Microbially Reduced Biotite and Chlorite. *Environ. Sci. Technol.* **2015**, 49, 13139-13148.
83. Gehin, A.; Greneche, J.M.; Tournassat, C.; Brendle, J.; Rancourt, D.G.; Charlet, L. Reversible surface-sorption-induced electron-transfer oxidation of Fe(II) at reactive sites on a synthetic clay mineral. *Geochim. Cosmochim. Ac.* **2007**, 71, 863-876.
84. Campbell, K.M.; Kukkadapu, R.K.; Peacock A.D.; Lesher, E.; Williams, K.H.; Bargar, J.R.; Wilkins, M.J.; Figueroa, L.; Ranville, J.; Davis, J.A.; Long, P.E. Geochemical,

mineralogical and microbiological characteristics of sediment from a naturally reduced zone in a uranium-contaminated aquifer. *Appl. Geochem.* **2012**, 27, 1499-1511.
85. Qafoku, N.P.; Gartman, B.N.; Kukkadapu, R.K.; Arey, B.W.; Williams, K.H.; Mouser, P.J.; Heald, S.M.; Bargar, J.R.; Janot, N.; Yabusaki, S.; Long, P.E. Geochemical and mineralogical investigation of uranium in multi-element contaminated, organic-rich subsurface sediment. *Appl. Geochem.* **2014**, 42, 77-85.
86. Ernstsen, V.; Gates, W.P.; Stucki, J.W. Microbial Reduction of Structural Iron in Clays—A renewable Source of Reduction Capacity. *J. Environ.Qual.* **1998**, 27, 761-766

Supporting information for**:**

Tc(VII) and Cr(VI) Interaction with Naturally Reduced Ferruginous Smectite from a Redox Transition Zone

*Odeta Qafoku[1], Carolyn I. Pearce[1], Anke Neumann[2], Libor Kovarik[3], Mengqiang Zhu[4], Eugene S. Ilton[1], Mark E. Bowden[3], Charles T. Resch[1], Bruce W. Arey[3], Elke Arenholz[5] , Andrew R. Felmy[6], Kevin M. Rosso[1]

[1]Pacific Northwest National Laboratory, P.O. Box 999, MS K8-96, Richland, Washington, 99352, U.S.A.

[2]Newcastle University, Newcastle, U.K.

[3]Environmental Molecular Sciences Laboratory, PNNL, U.S.A.

[4]University of Wyoming, Laramie, Wyoming, U.S.A.

[5]Lawrence Berkeley National Laboratory, Berkeley, California, U.S.A.

[6]Washington State University, Pullman Washington, U.S.A.

*Corresponding author: odeta.qafoku@pnnl.gov; Phone: + 509-371-6353; Fax: + 509-371-6354.

Number of pages 25

Number of Tables 7

Number of Figures 10

S1. Fractionation to clay-sized particles. The sediment (~10 g) was added to deionized water (2 L) and thoroughly mixed. Top 15cm of the slurry column was collected using a J-tube after the suspension was allowed to settle for 12 h during the first day and 8 h for the following 5 days. Each time after slurry collection, the suspension was replenished with de-ionized water to bring the volume to 2 L. All oxidized clay suspensions were combined, clear supernatant removed by pipetting to a final volume 1L that was further concentratedby air-drying to a reduced volume of ~ 250 mL. The suspension was then freeze dried. The anoxic clay suspensions were reduced to ~ 250 mL inside the N_2-chamber by freezing/thawing procedure. Lastly, the anoxic clay suspension was freeze-dried in vessels containing O_2-traps (Fe^0/Fe^{2+} enclosed mixtures).

S2. X-ray diffraction (XRD). The X-ray source is a long-fine-focus ceramic X-ray tube with a Cu anode. Quantitative compositions were determined by whole-pattern Rietveld fitting of the XRD patterns using TOPAS v4.2 (Bruker AXS). Data were collected at a 2θ range of 0 to 100° with a scan step of 0.01°, acceleration voltage of 50 kV, and beam current of 40 mA. The clay fractions after the removal of amorphous or poorly crystalline iron oxides following ascorbic acid extraction were also examined by XRD.

S3. Oriented Specimens preparation. The oriented specimens were prepared by quickly vacuum filtering the K- and Mg- clay suspensions through a membrane filter (Millipore 0.45 μm). The filtrate was gently inverted onto an aluminum slide and the filter membrane was removed to leave a homogeneous clay layer. Clay slides were equilibrated overnight at 30% relative humidity (saturated $MgCl_2$ solution) and at full humidity before and after solvation in ethylene glycol. The X-ray for basal reflections were collected by XRD over a 2θ range of 2 to 40º with 2 seconds intervals. Identification of the end-member of the dioctahedral smectite was resolved from preferred orientation XRD diffraction analysis. The large extent of expansion in the d_{001} spacing with increasing of the relative humidity (RH) and glycolation (Table S1) points toward montmorillonite as the dioctahedral smectite opposed to beidellite that would swell to a lesser degree due to layer charge located in the tetrahedral sheet.

S4. Acid digestion method for determining RTZ clay fraction chemical composition. To determine chemical composition, acid digestion of both the oxic and anoxic clay fractions was conducted in the N_2-chamber to avoid sample oxidation. All solutions were prepared with degassed and de-ionized water that was boiled under vacuum for 30 minutes followed by overnight N_2 sparging. The dissolved O_2 concentration in such solutions was measured to be <20 ppb. Ferrous ethylenediamine sulfate (standard grade) with known Fe(II)/(III) was used as the standard, while clay samples with known compositions such as smectite SWa-1, nontronite NAu-2 (Source Clays Repository of The Clay Minerals Society), and Panther Creek bentonite (American Colloid Company, Chicago, IL) were used as reference materials. After digestion, 1mL sample was fully reduced by addition of 1% Na-citrate and 1% $(NH_2OH)_2 \cdot H_2SO_4$ (10 mL). Concentration of Fe(II) in the original and reduced digests was measured by UV-vis (Shimadzu UV-2501 PC). Fe(III) content was calculated by difference. Total Fe, Si, Al, K, Mg, Ca, and Na concentration was measured by inductively coupled plasma optical emission spectroscopy (ICP-OES, Perkin Elmer Optima 2100).

S5. Cation exchange capacity (CEC), exchangeable cations, and Fe components. The type and concentration of exchangeable cations in clays was determined by extraction in 1M $NH_4CH_3CO_2$ at pH 7[1]. CEC was determined by saturating the clay sample (50 mg) in a mixture of CH_3COONa (0.4 M), NaCl (0.1 M), and ethanol (60%) at pH 8.2 followed by extraction in $Mg(NO_3)_2$ (0.5 M)[2] . The most reactive Fe(II) pool was determined after extraction (1 h) of anoxic clay in HCl (0.5 M)[3]. Poorly crystalline Fe components were determined after equilibration (24 h) of clay powders in ascorbate-citrate solution at pH 8.0 Clay fractions were also analyzed for inorganic carbon (Shimadzu 5000a) and organic carbon (Elementar Vario TOC cube).

S6. Extent of reduction of the RTZ oxidized clay fraction. Increments of bioreduced AH_2DS (5 mM), generated using *S.oneidensis* strain MR-1 in 10mM PIPES buffer (pH 7)[4] were added to 0.1 g clay suspension to produce a final volume of 10mL. After equilibration for 10 days in the dark the pH, Eh, solid Fe(II)/Fe(III), and aqueous AQDS/AH_2DS speciation were measured as follows. Suspension pH was determined using a combination glass electrode (Orion, ThermoScientific) while Eh was measured using a Pt band Broadley-James redox

electrode. To determine solid and aqueous species, aliquots of well mixed clay suspension (1.4 mL) were centrifuged at 13,000 rpm for 20 min. The precipitate was digested (see section 2.3) while the remaining solution was passed through pre-rinsed Whatman® VectaSpin 3 centrifuge tube filters (0.45 μm pore size). Fe(II) and Fe(III) content in the solid was determined as described in S4. Aqueous filtrate, transferred to 1 cm pathlength glass cuvette with an airtight Teflon seal screw top, was taken outside of N_2 anoxic chamber to measure AQDS/AH_2DS species with a Shimadzu UV-2501PC spectrometer. Absorbance data measured at 326 and 388 nm for respectively AQDS and AH_2DS were converted to concentration using the extinction coefficient (ε) values previously reported[5]. Lastly, a control sample without clay and with a known AH_2DS concentration was subjected to same experimental method described above to confirm that no sample oxidation occurred during the entire procedure.

S7. Extended X-ray absorption fine structure with linear combination fitting (EXAFS/LCF). For EXAFS analysis, each dried powder sample was mounted into a plastic cell sealed with Kapton window. Iron metal foil was measured concurrently with the samples for internal energy calibration (E_0 = 7112 eV). To prevent oxidation, reduced clay sample was mounted inside anaerobic glovebox prior to measurements, while Helium gas was purged into the sample chamber during the EXAFS data collection. Each scan took about 25 mins and 3 scans were collected per sample. Energy calibration and scan average were conducted using SixPack[6] with the Athena program[7] used for background removal, normalization, and extraction of EXAFS data. Sediment samples typically contain a mixture of multiple Fe species therefore EXAFS shell-by-shell fitting analysis is unable to identify and quantify each Fe species. LCF fitting was performed by a least-squares combination of EXAFS spectra of relevant Fe-bearing reference solids, including nontronite, vermiculite, Fe-(oxy)hydroxides, and ferrous compounds such as pyrite and siderite. For the oxic clay experimental spectra fitting indicates that vermiculite, nontronite, and ferrihydrite are required to ensure a good LCF fit (Figure 3). Known Fe species were tested for the LCF analysis, including Fe-bearing clay minerals, Fe oxides and oxyhydroxides, and ferrous iron compounds (pyrite and siderite). For the reduced clay only a combination of vermiculite and

nontronite is needed to match the measured EXAFS spectrum although the fit was improved marginally by pyrite addition.

S8. X-ray absorption spectroscopy (XAS) spectral fitting. The spectral resolution for the XAS data was sufficient to fit two peaks in the Fe L_3 region equivalent to crystallographic sites for Fe d6Oh (~710 eV) and Fe d5 Oh (~712 eV). Powders were pressed into iridium foil attached to a copper measurement probe using silver paint to improve conductivity. To obtain the cation distribution over the Fe sites, the experimental XAS spectra were fitted by means of a nonlinear least-squares analysis, using the calculated spectra for each site[8,9]; the 10Dq crystal field parameters were taken as 1.4 eV for Fe Oh sites. The intensity ratio between the two L_3 peaks was not perfectly reproduced by the calculated spectra, with the intensity of the leading peak too low in the calculation[9,10]. Further experimental and spectrum fitting details can be seen elsewhere[11].

S9. Mössbauer spectroscopy and Spectral fitting. Reduced clay samples for Mössbauer analysis were sealed between two pieces of Kapton tape to avoid oxidation. Mössbauer spectra center shift is reported with reference to α-Fe(0) foil. Voigt-based fitting[12] , as implemented in the software Recoil (Ottawa, Canada), was used to derive the Mössbauer parameters from the experimental data. The spectra were fit using the least number of spectral components possible. When adding an additional spectral component, the statistical significance of the additional phases was assessed by a) an improved overall goodness of fit ($\chi 2$) for the case including the phase in question vs. excluding the component, and b) the obvious presence of an additional phase when fitting the spectrum without this phase. The Fe(III) spectral feature was fit with two individual components, with hyperfine values characteristic for octahedral Fe(III) (Table S3). While the quadrupole split value of the main component Oct_1 Fe(III) (76% of the spectral area) is consistent with octahedral Fe(III) in many phyllosilicates, the large quadrupole split observed for Oct_2 Fe(III) (20% of the spectral area) is often associated with octahedral Fe(III) in a distorted binding geometry[13] and outside the range expected for quadrupole split values in iron sulfides such as pyrite[14]. In addition to the Fe(III) components, a third component consistent with octahedral Fe(II) had to be included in the fit (red doublet in Figure S5, A), which comprises almost 3.5% of the spectral

area and is consistent with digestion results that showed 4.6% Fe(II) in the oxic clay fraction. The presence of octahedral Fe(II) could be due to trioctahedral regions in the dioctahedral montmorillonite, that are stable even in an oxidized environment.

S10. Scanning electron microscopy with energy dispersive spectroscopy (SEM/EDS) and focused ion beam transmission electron microscopy (FIB-TEM) sample preparation and analysis. SEM elemental distribution mapping and EDS compositional analysis were performed on thin sections prepared by mixing freeze dried clay (~100 mg) with epoxy resin transferred into a 10mm base mount. After degassing and curing overnight under vacuum the dried mount was cut and polished into 4mm thin sections. The thin sections were carbon coated (10 nm) prior to SEM analysis. For TEM analysis, we initially identified the area of interest using SEM. Then a Pt layer ~0.5 μm followed by C layer ~3 μm were deposited for protecting sample integrity during ion beam milling. Gallium ion beam was used to prepare an electron transparent wedge with < 100 nm in thickness which was mounted into a TEM Cu grid.

S11. Tc(VII) and Cr(VI) analysis from the reactivity with RTZ anoxic clay. Reduction experiments were conducted in glass serum bottles (30 mL) sealed with rubber stoppers and crimp seals. An aliquot of 6.16 mM Tc(VII) (NH_4TcO_4, Perking Elmer) or 6.16 mM Cr(VI) (Na_2CrO_4, Sigma Aldrich) was added to the well-suspended clay to achieve concentrations of 2.5 μM and 10 μM for Tc(VII) and, 2.5 μM and 50 μM for Cr(VI). Following addition, the suspensions were hand shaken periodically and at each sampling time. Samples were analyzed for Tc(VII) or Cr(VI) several times during the duration of the experiments and pH values were monitored periodically. Sampling consisted into removing 2 mL clay suspension and filtering through 0.22 μm PVDF syringe filters (Fisher Scientific). An 1 mL filtrate was mixed with 9mL PerkinElmer scintillation cocktail and the mixture was analyzed for Tc(VII) by counting 99Tc activity for 10 min in a liquid scintillation counter (Packard 2500TR). For 2.5 μM Cr(VI) experiments, 1mL filtrate was acidified and analyzed with ICP-OES for while for 50 μM Cr(VI) experiments 1 mL filtrate was mixed with diphenylcarbizide and the absorbance of Cr(VI) complex was measured at 540nm with UV-vis spectrometer[14] (Shimadzu UV-2501 PC). Control experiments in absence of clay

confirmed no loss of Tc(VII) or Cr(VI) due to adsorption to glass bottles or syringe filters. At 2 months, post-reaction solids were separated by centrifugation, rinsed with deionized water, and freeze-dried or dried under N_2 for characterization (SEM/EDS, XMCD, FIB-TEM). To investigate homogeneous reduction kinetics 10 μM Tc(VII) was reacted with 30 μM Fe(II) and 50 μM Cr(VI) was reacted with 150 μM Fe(II) in absence of the solid phase.

REFERENCES:

1. Thomas, G.W. Exchangeable Cations. In *Methods of Soil Analysis, Part 2: Chemical and Microbiological Properties*; Page, A.L., Miller, R.H., Keeney, D.R. Eds.; American Society of Agronomy Inc. and Soil Science Society of America, Inc.: Wisconsin 1982; pp. 159
2. Rhoades, J.D. Cation Exchange Capacity. In *Methods of Soil Analysis, Part 2: Chemical and Microbiological Properties*; Page, A.L., Miller, R.H., Keeney, D.R. Eds.; American Society of Agronomy Inc. and Soil Science Society of America, Inc.: Wisconsin 1982; pp. 149
3. Peretyazhko, T.S.; Zachara, J.M.; Kukkadapu, R.K.; Heald, S.M.; Kutnyakov, I.V.; Resch, C.T.; Arey, B.W.; Wang, C.M.; Kovarik, L.; Phillips, J.L.; Moore, D.A. Pertechnetate (TcO_4^-) reduction by reactive ferrous iron forms in naturally anoxic, redox transition zone sediments from the Hanford Site, USA. *Geochim. Cosmochim. Ac.* **2012**, 92, 48-66.
4. Liu, C., Zachara, J.M., Foster, N.S. and Strickland, J. (2007) Kinetics of reductive dissolution of hematite by bioreduced anthraquinone-2,6-disulfonate. *Environ. Sci. Technol.* **41**, 7730-7735.
5. Ma, J.H., Del Vecchio, R., Golanoski, K.S., Boyle, E.S. and Blough, N.V. (2010) Optical Properties of Humic Substances and CDOM: Effects of Borohydride Reduction. *Environ. Sci. Technol.* **44**, 5395-5402.
6. Webb, S. M., SIXpack: a graphical user interface for XAS analysis using IFEFFIT. *Phys. Scripta* **2005,** *T115*, 1011-1014
7. Ravel, B.; Newville, M., ATHENA, ARTEMIS, HEPHAESTUS: data analysis for X-ray absorption spectroscopy using IFEFFIT. *J. Synchrotron Radiat.* **2005**, 12, (4), 537-541.
8. Vanderlaan, G.; Thole, B.T. Strong Magnetic-X-Ray Dichroism in 2p Absorption-Spectra of 3d Transition-Metal Ions. *Phys. Rev. B* **1991**, 43, 13401-13411.
9. Vanderlaan, G.; Kirkman, I.W. The 2p Absorption-Spectra of 3d Transition-Metal Compounds in Tetrahedral and Octahedral Symmetry. *J Phys-Condens. Mat.* **1992**, 4, 4189-4204.
10. Crocombette, J.P.; Pollak, M.; Jollet, F.; Thromat, N.; Gautiersoyer, M. X-Ray-Absorption Spectroscopy at the Fe L(2,3) Threshold in Iron-Oxides. *Phys. Rev. B* **1995**, 52, 3143-3150.
11. Pearce, C.I.; Liu, J.; Baer, D.R.; Qafoku, O.; Heald, S.M.; Arenholz, E.; Grosz, A.E.; McKinley, J.P.; Resch, C.T.; Bowden, M.E.; Engelhard, M.H.; Rosso, K.M.

Characterization of natural titanomagnetites ($Fe_{3-x}Ti_xO_4$) for studying heterogeneous electron transfer to Tc(VII) in the Hanford subsurface. *Geochim. Cosmochim. Ac.* **2014**, 128, 114-127.
12. Rancourt, D.G.; Ping, J.Y. Voigt-Based Methods for Arbitrary-Shape Static Hyperfine Parameter Distributions in Mossbauer-Spectroscopy. *Nucl. Instrum. Meth. B* **1991**, 58, 85-97.
13. Dyar, M.D.; Agresti, D.G.; Schaefer, M.W.; Grant, C.A.; Sklute, E.C. Mossbauer spectroscopy of earth and planetary materials. *Annu. Rev. Earth Pl. Sc.* **2006**, 34, 83-125.
14. Nishihara, Y.; Ogawa, S., Mössbauer study of ^{57}Fe in the pyrite-type dichalcogenides. *The Journal of Chemical Physics* **1979,** *71*, 3796-3801.
15. American Public Health Association (APHA) Standard methods for the examination of water and wastewater. 20th ed. American Public Health Association, American Water Works Association, 1998, Water Environment Federation, APHA, Washington, D.C.

Table S1. Mineralogical components and phase quantification determined by Rietvield refinement using external ZnO as a standard

RTZ Horizon	Clay Size Fraction (% of whole sediment)	Clay minerals (%)		Minor phases (%)			
		*Smectite	Kaolinite	Albite	Quartz	Anorthoclase	Cristobalite
Oxidized 18 – 18.3 m	6.1	84	5	2	1	1	1
Reduced 18.6 – 18.9 m	8.6	82	12	2	2	1	1

* Smectite values are somewhat overestimated due to presence of unquantifiable amorphous component that appeared to be more significant in the anoxic fraction. Uncertainty for the amount of oxidized smectite is 5% and for the amount of reduced smectite is 6%, calculated based on the sum of uncertainties for remaining crystalline phases.

Table S2. The extent of reduction of native oxic clay determined using anthraquinone 2,6 disulfonic acid (AQDS) as an electron mediator. Results show that maximum reducible Fe by AH_2DS in oxidized clay approximates to 24% $Fe(II)/Fe_{Total}$

added AH_2DS	pH	pe	measured				% reduction
			AQDS	AH_2DS	Fe(II)	Fe(III)	
mmol/L			mmol/L		mmol/g clay		
0.5	6.90	4.02	0.49	0.01	0.099	1.168	7.8
1	6.85	-0.65	0.95	0.03	0.153	1.155	11.7
1.5	6.91	-1.94	1.40	0.09	0.224	1.076	17.3
2	6.93	-2.62	1.69	0.35	0.270	1.043	20.6
2.5	6.88	-2.89	1.74	0.79	0.278	0.989	21.9
3	6.90	-3.00	1.82	1.21	0.270	0.931	22.5
3.5	6.96	-3.10	1.85	1.59	0.287	0.958	23.1
4	6.97	-3.16	2.02	2.03	0.309	0.982	23.9

Table S3: Mössbauer parameters for fitted spectra of oxic and anoxic clay fractions from the RTZ, Hanford site. [a]Center shift relative to α-Fe(0). [b]Quadrupole splitting. [c]Standard deviation.

Sample (χ^2)	component	CS[a] (mm/s)	QS[b](σ)[c] (mm/s)	area(σ)[c] (%)
Oxic, 290 K (0.81)	Oct_1 Fe(III)	0.37	0.43(0.26)	76.9(0.7)
	Oct_2 Fe(III)	0.40	1.22(0.47)	19.1(0.6)
	Fe(II)	1.05	2.59(0.23)	3.9(0.5)
Oxic, 14 K (0.87)	Oct_1 Fe(III)	0.48	0.45(0.28)	76.0(0.5)
	Oct_2 Fe(III)	0.46	1.25(0.45)	20.6(0.4)
	Fe(II)	1.26	2.71(0.26)	3.4(0.4)
Reduced, 18K (2.05)	Oct_1 Fe(III)	0.47	0.47(0.28)	61.5(0.6)
	Oct_2 Fe(III)	0.48	1.34(0.55)	20.6(0.5)
	Fe(II)	1.28	2.83(0.27)	17.9(0.4)

Table S4: The d-spacing of Mg- and K- saturated oxic clay displaying large swelling properties. The extent of expansion in the d_{001} spacing is indicative of montmorillonite as the dominant mineralogical component.

Oxidized Clay	d-spacing (Å)		
	Random orinetation RT*	Basal Orientation	
		30% RH**	full H_2O saturation
Mgsat	14.42	15.28	19.79
Mgsat. glycolated	n.a.	16.75	21.05
Ksat	12.23	12.93	16.07
Ksat glycolated	n.a.	14.36	17.09

*Room temperature

**Relative Humidity

Table S5: Tabulation of Fe species tested in the EXAFS linear combination analysis and the linear combination fitting (LCF) in RTZ clay fractions

	Ferrihydrite	**Vermiculite**	**Nau2Red10**	**R**	**Reduced χ^2**
OxiSed	0.16 ± 0.03	0.46 ± 0.03	0.38 ± 0.02	0.021	0.195
RedSed	---	0.68 ± 0.03	0.32 ± 0.02	0.032	0.250

Table S6: Tabulated EXAFS parameters for the nearest O-shell in RTZ clay fractions

Samples	***R***	**Shell**	**CN**	**Dist(Å)**	**σ^2**	**ΔE(ev)**
Vermiculite	0.0007	Fe-O	5.3(3)	2.014(4)	0.009(1)	0.6(7)
Nau2Red10	0.0016	Fe-O	5.5(5)	2.005(6)	0.003(3)	0(1)
RedSed	0.0001	Fe-O	5(1)	2.02(2)	0.006(2)	0(3)
OxSed	0.0035	Fe-O	5.8(8)	2.00(1)	0.006(6)	2(2)

Table S7: HCl extraction at pH ~4 of RTZ anoxic clay before and after Fe(II) sorption showing insignificant changes in aqueous concentration after the Fe(II) uptake.

RTZ Anoxic Clay fraction	24h HCl extraction[a]	
	native	post 0.150 mM Fe(II) sorption (Fe(II) added = 19.7 µmol/g clay)
pH	~ 4	~ 4
Fe^{2+}(µmol/g)	7.66	8.08
Total $_{aq}$Fe (µmol/g)	8.01	8.85
Mg^{2+} (µmol/g)	44.33	44.03
Ca^{2+} (µmol/g)	114.36	107.81
K^{+} (µmol/g)	25.54	29.76
Na^{+} (µmol/g)	9.97	7.86

[a]Suspension density 7.6g/L

Figure S1. The XRD pattern and mineralogy of clay size fraction (< 2 μm) separated by sedimentation from whole oxidized and reduced sediment. Reflection at 62° 2θ that correspond to d_{060} spacing is representative of a dioctahedral smectite. The external standard ZnO reflections are greyed out for clarification.

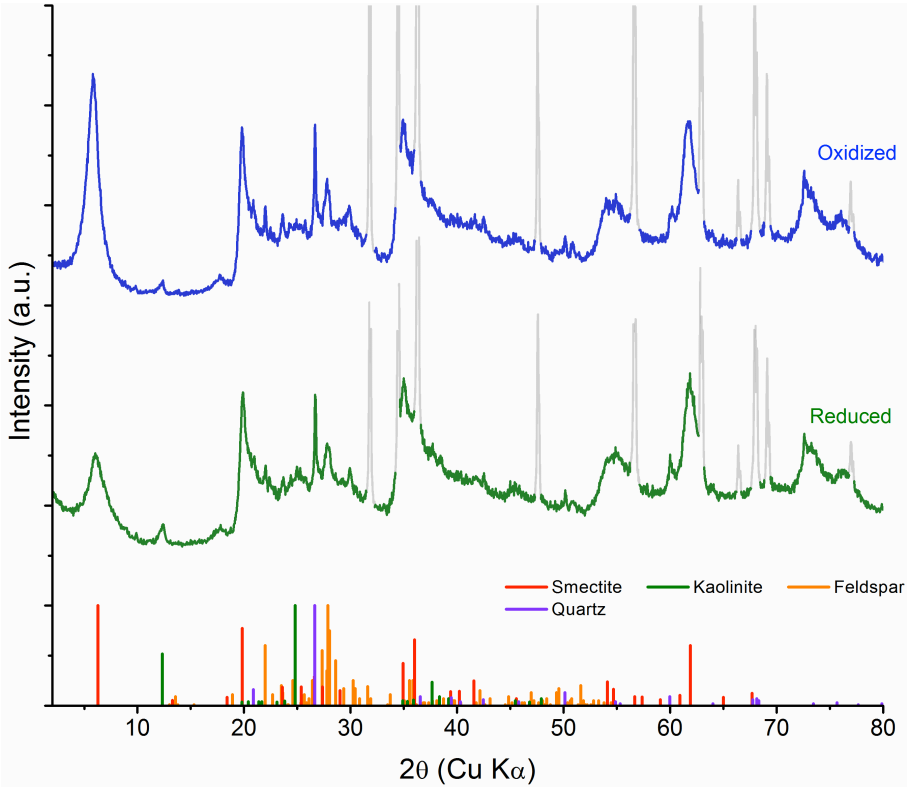

Figure S2. Backscattering SEM micrographs of RTZ anoxic clay showing high Z-contrast crystallites with cubic to octahedral equant morphologies incorporated into clay matrix. The particles were composed of Fe and S with a ratio varying from 1:1.6 to 1:1.1.

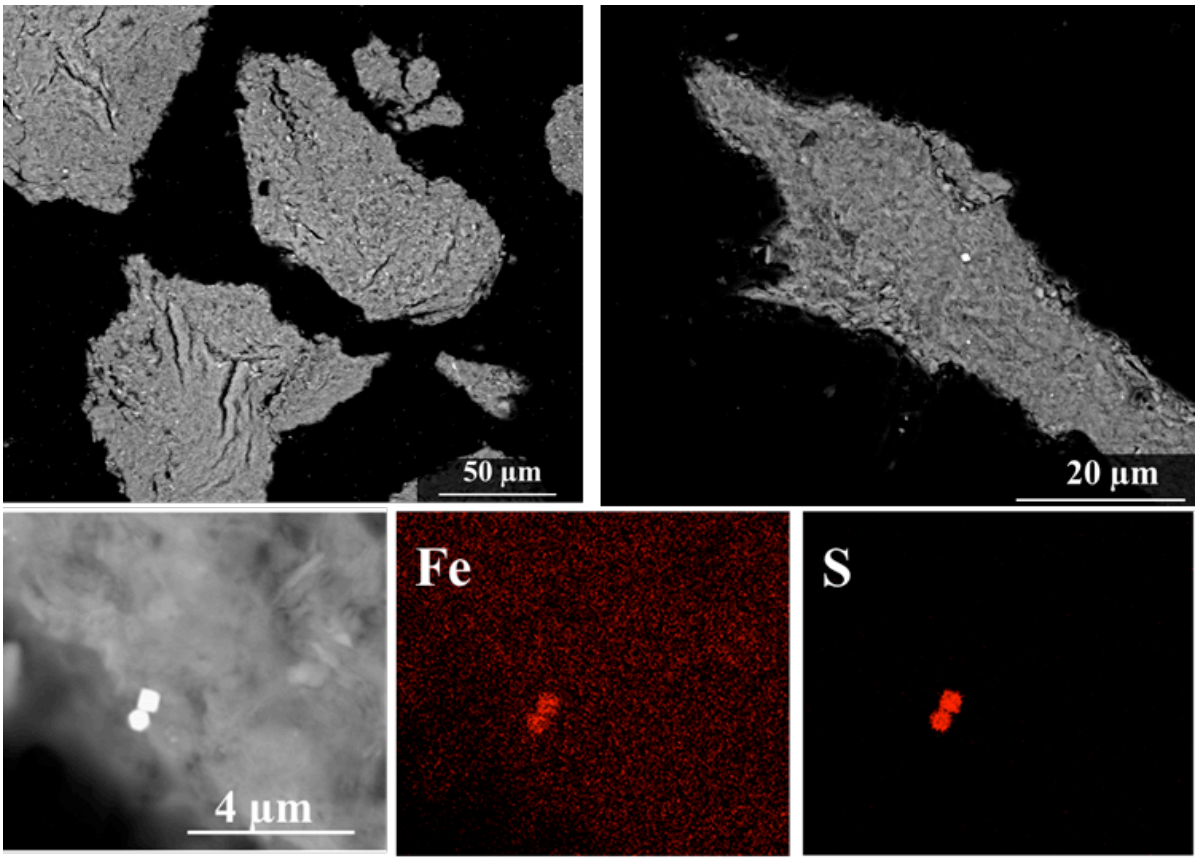

Figure S3. EXAFS spectra of the Fe species tested in the linear combination analysis and the linear combination fitting (LCF) analysis of Fe species in RTZ clay fractions

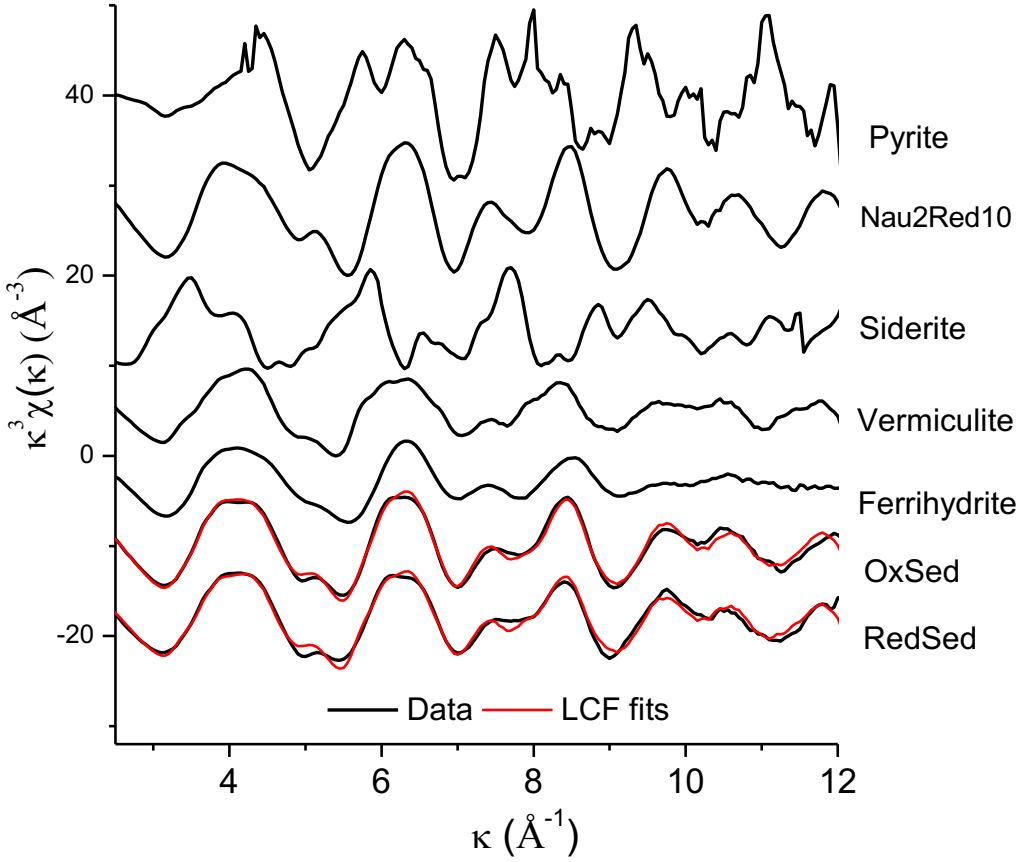

Figure S4. Comparison of fitted EXAFS spectra to the experimental data for the nearest O shell.

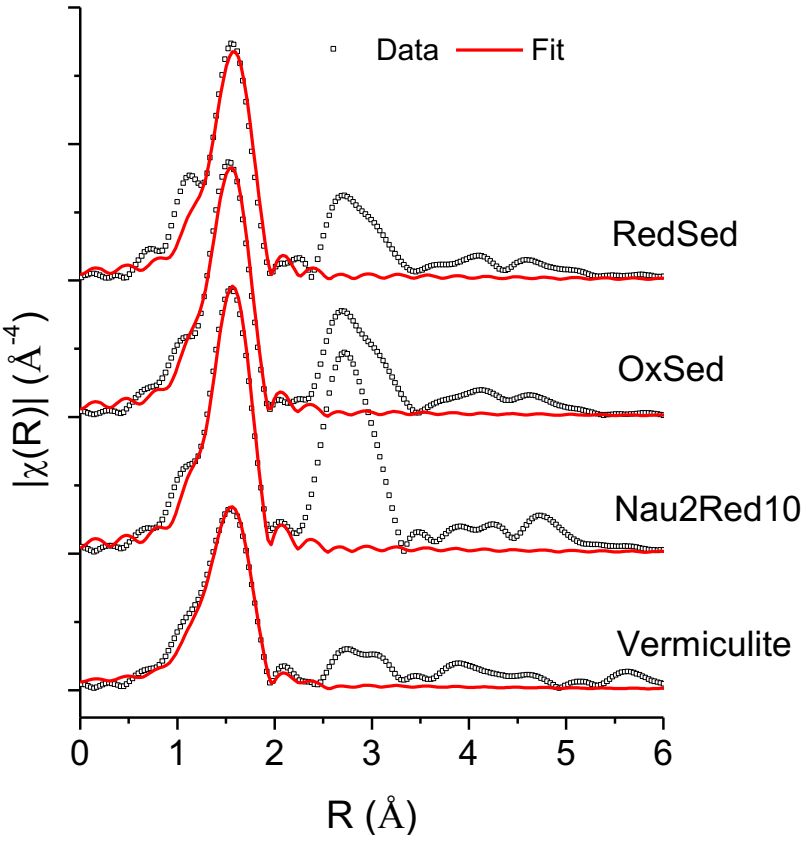

Figure S5: Room temperature Fe *L*-edge XAS showing: (a) similarities between the oxidized RTZ clay fraction and the oxidized Fe-clay standard (nontronite NAu-2); (b) data and fit for oxic clay XAS with 0.06 Fe(II) and 1.27 Fe(III) in octahedral coordination; (c) similarities between the reduced RTZ clay fraction and the reduced Fe-clay standard (nontronite NAu-2), the spectra of reduced RTZ clay falls between that of 10% and 100% reduced NAu-2; and (d) data and fit for reduced clay XAS with 0.28 Fe(II) and 1.05 Fe(III) in octahedral coordination

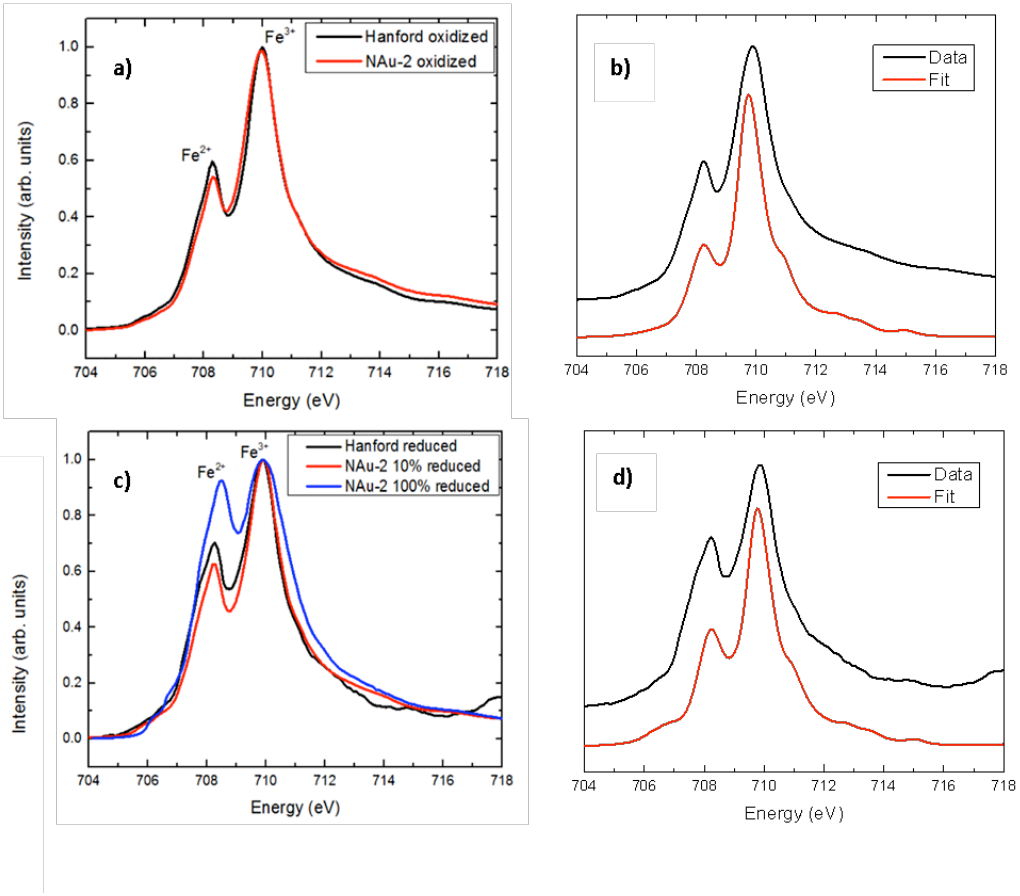

Figure S6: ^{57}Fe-Mössbauer spectra of oxic (A) and reduced (B) clay fractions from RTZ at Hanford site. The data were fitted with two octahedral Fe(III) clay mineral-bound components and one octahedral Fe(II) component, which occupies 3% and 18% of the spectral area for the oxic and reduced clay sample, respectively.

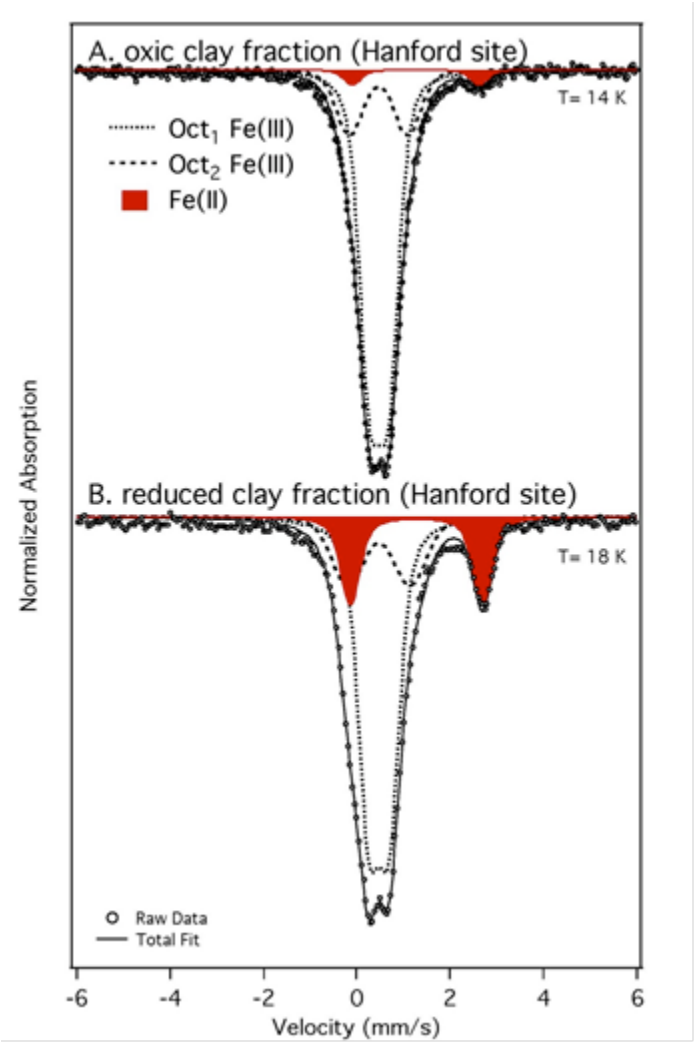

Figure S7. CrFe rich particles formed at ~50d post reaction of 50 µM Cr(VI) and anoxic clay pre-equilibrated with 150 µM Fe(II): (a) SEM left to right, compositional mapping; (b) FIB-TEM diffraction pattern of CrFe particles showing that the micron-size particle is composed of individual 10-50 nm crystallites, with electron diffraction displaying a ring pattern corresponding to random orientation of crystallites.

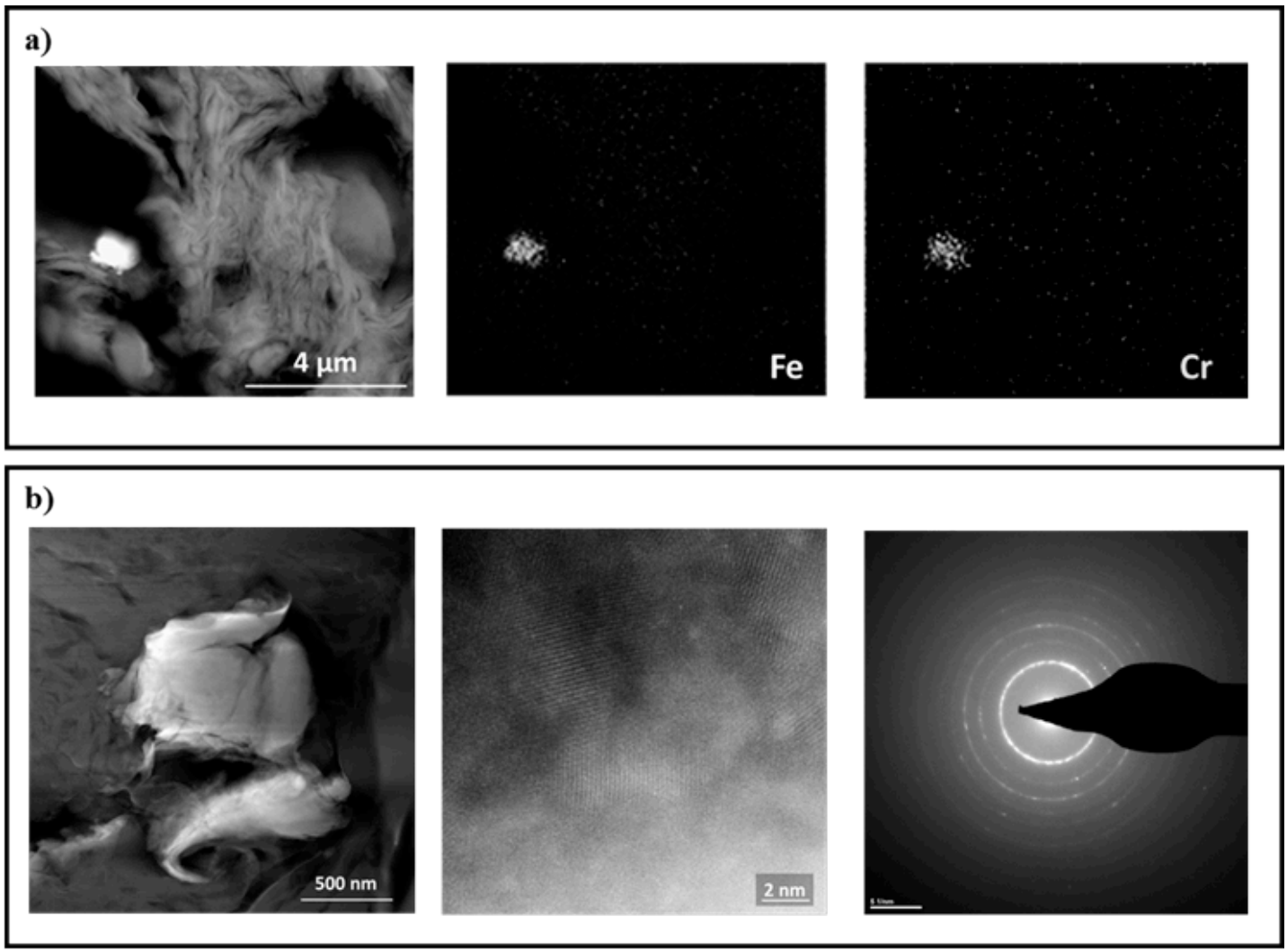

Figure S8. CrFe rich precipitates sampled at 30 minutes post-reaction between 50 µM Cr(VI) and 150 µM Fe(II) (in absence of solid phase). The SEM (a, b) and TEM (c, d) data reveal that the precipitate that formed during homogeneous reaction is of amorphous nature based on the diffused rings of TEM diffraction pattern.

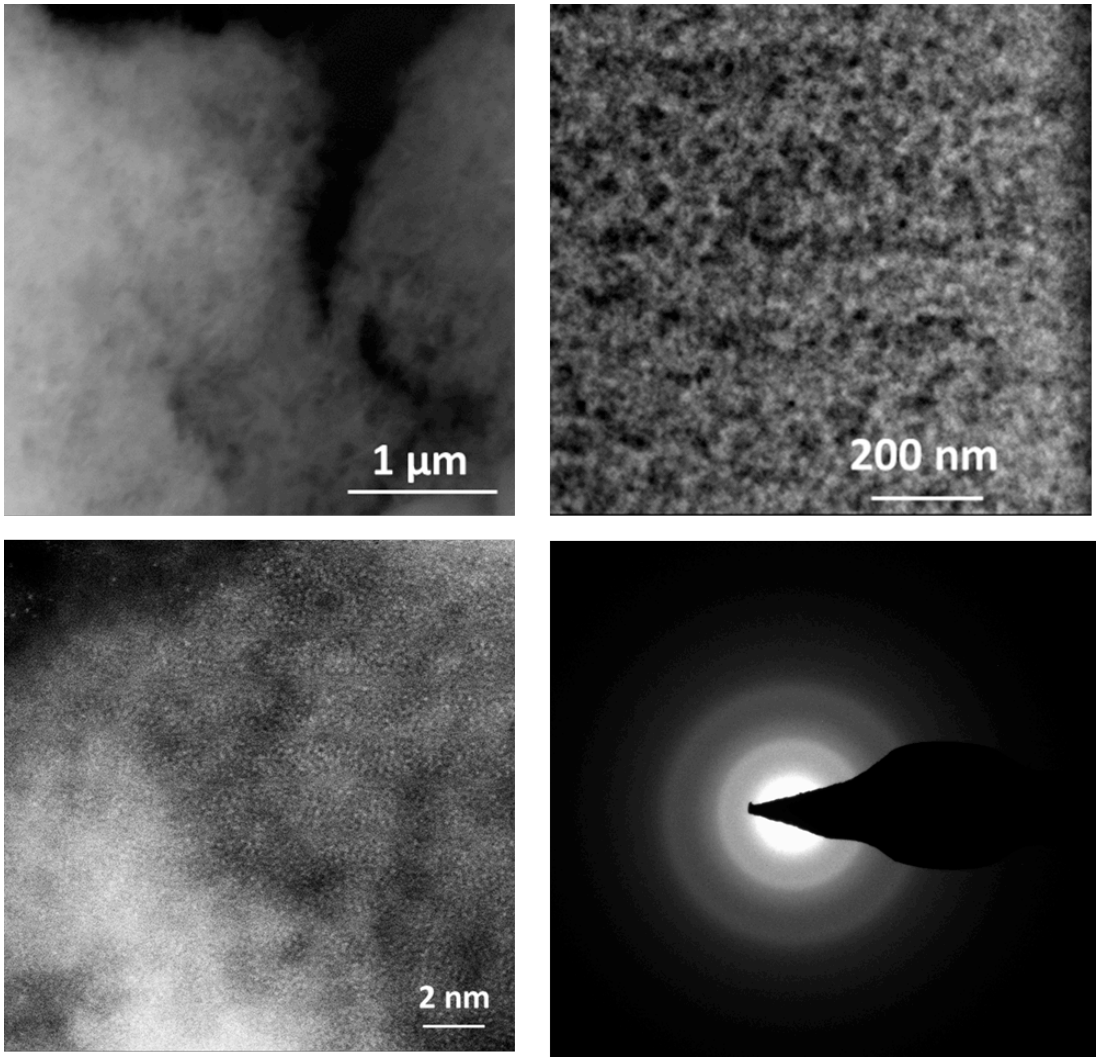

Figure S9: XAS of CrFe rich precipitate sampled at 30 minute post-reaction between 50 µM Cr(VI) and 150 µM Fe(II): (a) Fe *L*-edge, (b) O *K*-edge and (c) Cr *L*-edge. The data reveal that solid formed during homogeneous precipitation is composed of goethite-like Cr(III)-Fe(III) rich particles. [14]

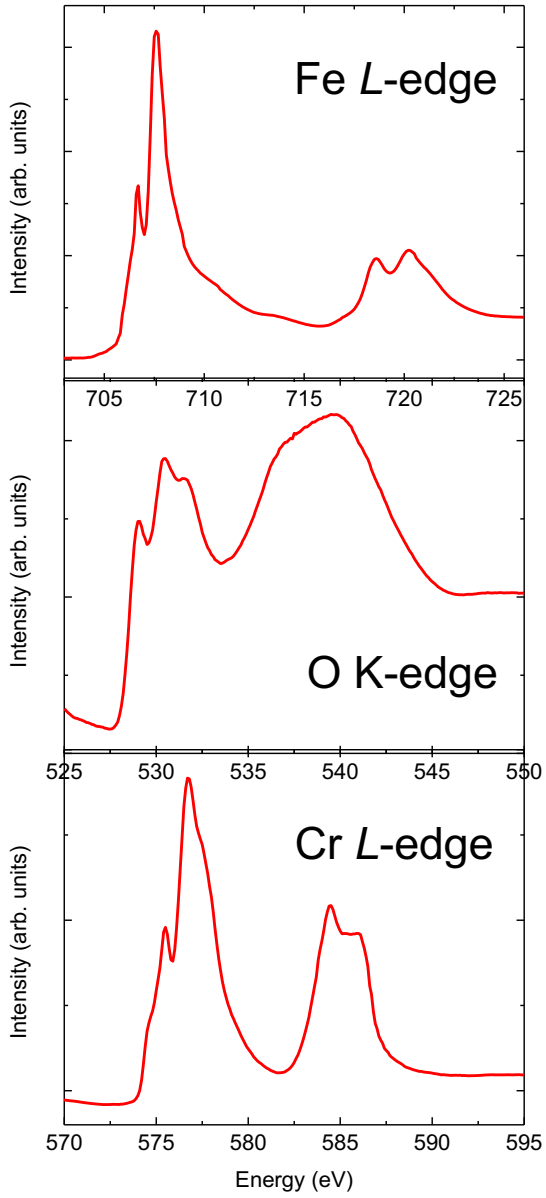

Figure S10: Post reaction samples of RTZ anoxic clay pre-equilibrated with 150 µM Fe(II) and reacted for ~50d with 50 µM Cr(VI): (a) SEM micrograph of clay particles dried under N_2 (no centrifugation); (b, c) SEM micrograph of clay particles after centrifugation showing significant aggregation and formation of large clay particles.